Science of the Total Environment 924 (2024) 171681

Contents lists available at ScienceDirect

Science of the Total Environment

journal homepage: www.elsevier.com/locate/scitotenv

Neurotoxic effects of polystyrene nanoplastics on memory and microglial activation: Insights from *in vivo* and *in vitro* studies

Yunn Me Me Paing [a], Yunkyung Eom [a], Gyeong Bae Song [b], Bokyung Kim [b], Myung Gil Choi [b], Sungguan Hong [b,*], Sung Hoon Lee [a,*]

[a] College of Pharmacy, Chung-Ang University, Seoul 06974, Republic of Korea
[b] Department of Chemistry, Chung-Ang University, 84 Heukseok-ro, Dongjak-gu, Seoul 06974, Republic of Korea

HIGHLIGHTS

- Oral ingestion of nanoplastics (30–50 nm) induces memory impairment in adult mice.
- Microglia preferentially uptake nanoplastics among brain cells.
- Nanoplastic uptake induces microglial activation and inflammatory responses.
- Activated microglia by nanoplastics dysregulate hippocampal neuronal activity.
- Nanoplastics are potential environmental precipitants of cognitive impairment.

GRAPHICAL ABSTRACT

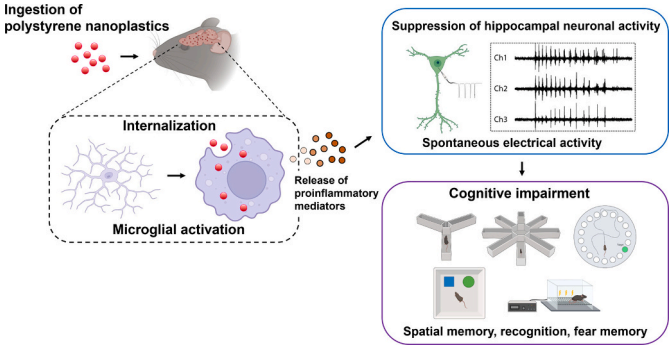

ARTICLE INFO

Editor: Henner Hollert

Keywords:
Polystyrene nanoplastics
Cognitive deficits
Microglia
Internalization
Neuroinflammation

ABSTRACT

Nanoplastics, arising from the fragmentation of plastics into environmental pollutants and specialized commercial applications, such as cosmetics, have elicited concerns due to their potential toxicity. Evidence suggests that the oral ingestion of nanoplastics smaller than 100 nm may penetrate the brain and induce neurotoxicity. However, comprehensive research in this area has been hampered by technical challenges associated with the detection and synthesis of nanoplastics. This study aimed to bridge this research gap by successfully synthesizing fluorescent polystyrene nanoplastics (PSNPs, 30–50 nm) through the incorporation of IR-813 and validating them using various analytical techniques. We administered PSNPs orally (10 and 20 mg/kg/day) to mice and observed that they reached brain tissues and induced cognitive dysfunction, as measured by spatial and fear memory tests, while locomotor and social behaviors remained unaffected. *In vitro* studies (200 μg/mL) demonstrated a predominant uptake of PSNPs by microglia over astrocytes or neurons, leading to microglial activation, as evidenced by immunostaining of cellular markers and morphological analysis. Transcriptomic analysis indicated that PSNPs altered gene expression in microglia, highlighting neuroinflammatory responses that may contribute to cognitive deficits. To further explore the neurotoxic effects of PSNPs mediated by microglial activation, we measured endogenous neuronal activity using a multi-electrode array in cultured hippocampal neurons. The application of conditioned media from microglia exposed to PSNPs suppressed neuronal activity, which was reversed by inhibitors of microglial activation. Our findings offer detailed insights

* Corresponding authors.
E-mail addresses: sungguanhong@cau.ac.kr (S. Hong), sunghoonlee@cau.ac.kr (S.H. Lee).

https://doi.org/10.1016/j.scitotenv.2024.171681
Received 30 October 2023; Received in revised form 5 March 2024; Accepted 10 March 2024
Available online 13 March 2024

into the mechanisms by which nanoplastics damage the brain, particularly emphasizing the potential environmental risk factors that contribute to cognitive impairment in neurodegenerative diseases.

1. Introduction

Plastic products are widely manufactured and used across commercial, industrial, and domestic sectors. Once discarded, these plastics degrade into smaller fragments, specifically microplastics (<5 mm in diameter) and nanoplastics (<1 μm in diameter), termed secondary microplastics and nanoplastics. These have been detected in oceans, rivers, soils, and sediment layers (Barnes et al., 2009; de Sa et al., 2018; do Sul and Costa, 2014). Additionally, microplastics and nanoplastics are produced for commercial products or industrial applications, known as primary microplastics and nanoplastics, including materials for research, drug delivery particles, cosmetics, and cleansers (Banerjee and Shelver, 2021). These particles are resistant to biodegradation and accumulate within the food web (Setala et al., 2014; Steer et al., 2017). Human exposure to these particles can occur through ingestion of contaminated food and water, direct use of plastic products, and inhalation of polluted air (Bouwmeester et al., 2015; Grodzicki et al., 2021; Pivokonsky et al., 2018; Waring et al., 2018). Once internalized, micro- and nanoplastics can circulate systemically and deposit in various organs, such as the liver, stomach, lungs, and spleen (Ding et al., 2018; Yong et al., 2020; Yu et al., 2018).

Nanoplastics are pervasive in the natural environment, including the atmosphere, soil, and seawater, and are more prevalent than microplastics (Ferreira et al., 2019; Gigault et al., 2018). They are also found in personal care products. There is growing concern over the adverse effects of nanoplastics, which, due to their small volume and large surface area, may preferentially interact with cellular membranes and structures, leading to severe toxicity. Nonetheless, the biological and ecological implications of nanoplastics are constrained by the limited availability of nanosized plastic materials and the technical challenges associated with the reliable detection and analysis of synthesized nanoplastics (Harrison et al., 2012; Merdy et al., 2023).

The neurotoxic effects of nanoplastics have been extensively investigated in marine invertebrates and fish, including species such as *Caenorhabditis elegans*, earthworms, zebra mussel, Mediterranean mussel, and zebrafish (Prust et al., 2020). These studies have demonstrated that exposure can lead to behavioral impairments and disruptions in cholinergic activity, often accompanied by oxidative stress. However, the impact of nanoplastics on rodent brains is still debated. While chronic oral exposure to nanoplastics did not result in significant changes in mouse behavior, including cognitive function assessed by Y-maze and passive avoidance tests, as well as locomotor activity evaluated by open field and rotarod tests (Rafiee et al., 2018), other research has indicated that exposure to metal nanoparticles impaired cognitive function in adult mice as measured by the novel object recognition test (NORT) (Estrela et al., 2021; Lee et al., 2023a). Moreover, maternal exposure to nanoplastics has been associated with neurophysiological and cognitive deficits in offspring, as determined by Y-maze and NORT (Jeong et al., 2022). Nanoplastics accumulation in the prefrontal cortex has been linked to reduced neuronal arborization (Suman et al., 2024), and they pose a potential risk for Parkinson's disease by decreasing ATP-related genes and proteins (Liang et al., 2022). A recent study suggested that oral ingestion of nanoplastics impaired brain behaviors and immunity through activation of the intestinal IL-1 signaling pathway, potentially implicating the gut-brain axis in brain dysfunction caused by nanoplastics (Lee et al., 2023b; Yang et al., 2023). However, the underlying toxic mechanisms of nanoplastics in the brain remain largely unexplored.

Fluorescent microplastics and nanoplastics beads are frequently used to track plastic distribution in tissues and to elucidate specific toxic mechanisms. However, issues such as fluorescent dye leaching from unconjugated nanoparticles or dye-specific interactions on cellular surfaces can create artifacts when investigating the biological effects of nanoplastics (Schur et al., 2019). Additionally, photobleaching or quenching of fluorescent dyes can impede the observation of plastic translocation and accumulation in tissues (Nikolic et al., 2022). Therefore, labeling nanoplastics by incorporating fluorescent dyes within the plastics offers several advantages, including the ability to investigate specific interactions of nanoplastics, reduce artifacts, and minimize photobleaching and quenching. In this study, we synthesized spherical fluorescent polystyrene nanoplastics and examined their neurotoxic impact through both *in vivo* and *in vitro* analyses.

2. Materials and methods

2.1. Synthesis of pristine and PSNPs

Spherical polystyrene nanoplastics were synthesized following the procedure outlined in Fig. 1A, with minor modifications from a previous study (Nuruzatulifah et al., 2016). Initially, 146 mL of deionized (DI) water was added to a three-necked round-bottom flask. Sodium dodecyl sulfate (SDS, 2.48 g) was then dissolved in the DI water. Subsequently, 15.26 g of purified styrene monomer was introduced into the solution and stirred at 300 rpm for 30 min. Potassium persulfate (KPS, 0.15 g) was dissolved in 10 mL of DI water and added to the reaction mixture. The system was heated to 70 °C and stirred at 300 rpm for 12 h. The resulting polystyrene nanospheres (30–50 nm) were designated as pristine. For the fluorophore, IR-813 (0.1 g) was dissolved in 15 mL of ethanol and added to the reaction. After 1 h, the mixture was cooled in an ice bath, and 450 mL of ethanol was added. The precipitated product was collected by centrifugation at 10,000 rpm and washed five times with ethanol. The polystyrene nanoplastics containing IR-813 (30–50 nm) were termed PSNPs. Both pristine and PSNPs were aliquoted and stored as a powder. Prior to treatment, they were suspended in normal saline by vigorous shaking for 30 min using a vortex mixer.

2.2. Validation of pristine and PSNPs

2.2.1. In vivo fluorescence imaging

The fluorescence intensity of both pristine and PSNPs was measured using an *in vivo* fluorescence imaging system (FOBI, Cellgentek, Daejeon-si, Korea). The distribution of IR-813 and PSNPs in mouse tissues was assessed with the fluorescence *in vivo* imaging system after the behavioral analyses. Mice were anesthetized with isoflurane and euthanized prior to measurement. Fluorescence signals corresponding to IR-813 were detected in various tissues, including the brain, stomach, intestine, liver, kidney, and heart.

2.2.2. Scanning electron microscopy (SEM) imaging

SEM imaging was conducted using a field-emission scanning electron microscope (FE-SEM, Zeiss, Oberkochen, Germany). For SEM imaging preparation, 100 mg of either pristine or PSNPs were dispersed in 10 mL of ethanol and sonicated for 30 min. A 100 μL sample was then placed onto a silicon wafer and coated with platinum at a current of 3 mA for 180 s. SEM images were captured at an accelerating voltage of 3 kV.

2.2.3. Dynamic light scattering (DLS)

The hydrodynamic size distribution of the synthesized nanoplastics was analyzed using a DLS size analyzer (ELSZ-1000, Otsuka, Japan). The nanoplastics were resuspended in Milli-Q water and sonicated for 30 min in a water bath to enhance resuspension. Measurements were performed in triplicate at 25 °C, with three separate preparations of

nanoplastics.

2.2.4. Fourier-transform infrared spectroscopy (FTIR) measurements

FTIR measurements were conducted in the wavenumber range of 4000–500 cm^{-1}, using an FTIR-6600-FV spectrometer (Jasco, Tokyo, Japan). Samples were prepared as pellets by mixing with IR-grade KBr (Pike Technologies, Madison, WI, USA).

2.3. Animal care and treatment

Animal care and handling adhered to the National Institutes of Health Guide for the Care and Use of Laboratory Animals and the guidelines of the Institutional Animal Care and Use Committee of Chung-Ang University (Approval No. A2022015). A total of 50 male C57BL/6 J mice (aged 7 weeks, weighing 25–30 g) were obtained from DBL (Chungchungbuk-do, Korea). The mice were housed under standard laboratory conditions with a temperature of 22 ± 3 °C and a relative humidity of 50–60 %, subjected to a 12-h light/dark cycle, and had *ad libitum* access to water and food. After a week of habituation, the animals were randomly divided and treated with reagents (n = 7 for normal saline, n = 19 for IR-813 [7 for PSNPs, 6 for normal saline, 6 for pristine], n = 6 for 10 mg/kg/day of PSNPs, n = 6 for 20 mg/kg/day of PSNPs, n = 6 for 10 mg/kg/day of pristine, n = 6 for 20 mg/kg/day of pristine). Group sizes and animal numbers were determined by animal ethics, welfare, and statistical considerations. PSNP doses were based on a previous study (Jeong et al., 2022) and were orally administered to the mice once a day at doses of 10 and 20 mg/kg/day suspended in 200 μL of normal saline. Mice were treated with IR-813 or PSNPs for seven weeks and sacrificed in the eighth week for imaging analyses. Healthy mice were used for experiments, and behavioral assessments were conducted as shown in Fig. 2A. Normal saline (200 μL), IR-813 (20 mg/kg/day suspended in 200 μL of normal saline), and pristine (10 or 20 mg/kg/day suspended in 200 μL of normal saline) were orally administered to mice once daily for six weeks. During treatment and behavioral analyses, the mice were housed under laboratory conditions with free access to water and food, except during the radial maze test duration.

2.4. Behavior analyses

2.4.1. Y-maze test

Working spatial memory was assessed using the Y-maze test, as previously described (Katz and Schmaltz, 1980). The Y-maze consisted of three identical arms made of white acrylic, each measuring 40 × 14 × 4 cm, arranged at 120° angles. During the training trial, mice were placed in one arm with another arm blocked, allowing them to explore for 15 min. An hour later, for the test trial, mice had access to all three

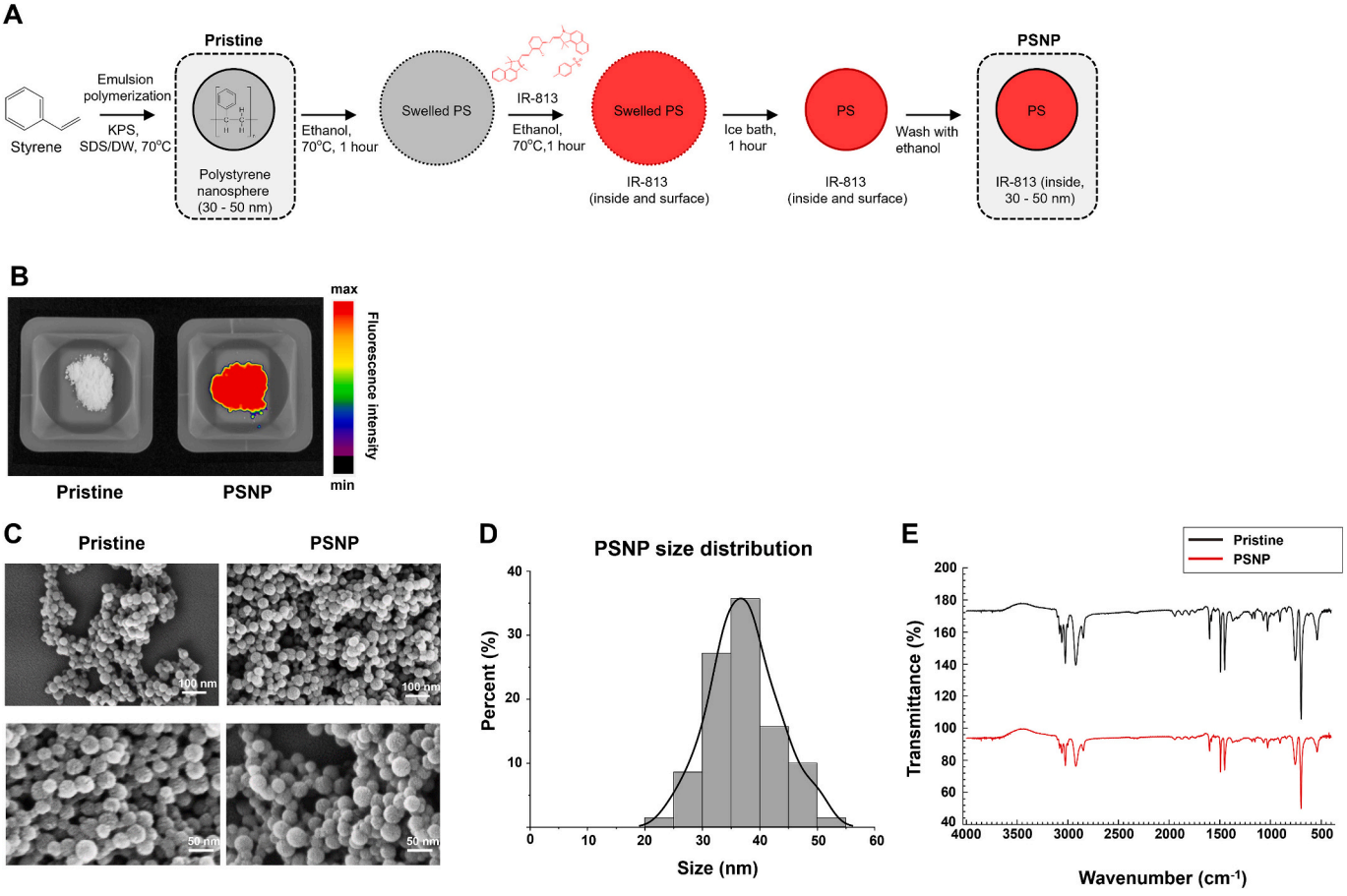

Fig. 1. Comprehensive analysis of PSNPs: Synthesis, characterization, and biodistribution of PSNPs following oral ingestion in mice.
(A) Schematic diagram illustrating the synthesis process of both pristine and PSNPs.
(B) Fluorescent imaging of pristine nanoparticles and PSNPs, using an *in vivo* fluorescence imaging system to detect the IR-813 signal. Comparative fluorescent imaging of both pristine nanoparticles and PSNPs using an *in vivo* fluorescence imaging system, highlighting the IR-813 signal distribution.
(C) High-resolution field-emission scanning electron microscopy (FE-SEM) images presenting a side-by-side morphological comparison of the surface textures and structural integrities of both the pristine and PSNPs.
(D) Size distribution curve of PSNPs as determined by dynamic light scattering (DLS).
(E) Fourier-transform infrared (FTIR) spectra of pristine (depicted in black) and PSNPs (depicted in red), demonstrating identical chemical structures with no discernible differences.

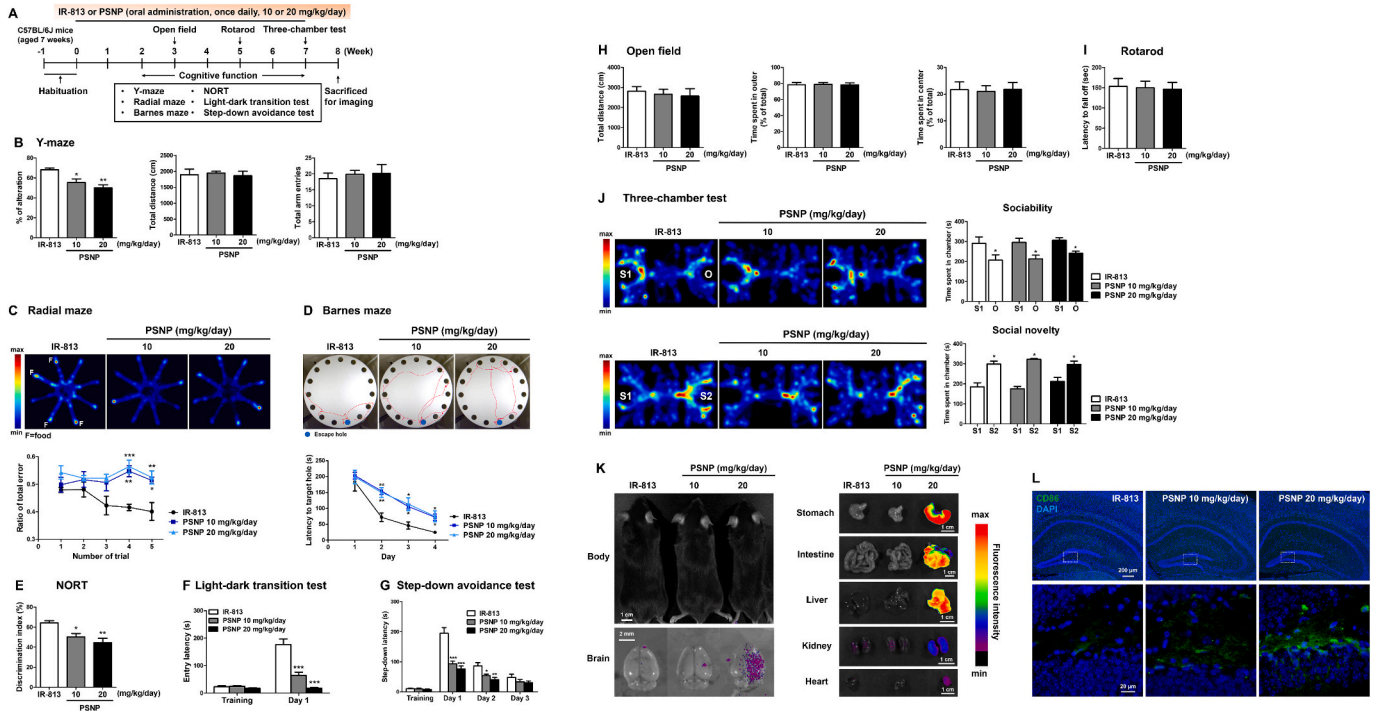

Fig. 2. Oral administration of PSNPs impairs learning and memory in mice.

(A) Experimental schedule for PSNP exposure and behavioral assessments. Mice received once daily oral administration of either IR-813 (20 mg/kg/day) or PSNPs (10 or 20 mg/kg/day) for a total of 7 weeks. Assessment of cognitive function during 2 to 7 weeks of exposure. Performance of open field, rotarod test, and three-chamber test at 3, 5, and 7 weeks of exposure, respectively. Sacrifice of mice at 8 weeks of exposure for *in vivo* imaging or immunohistochemical analyses.

(B) Y-maze results. Measurement of the percentage of alternation, total distance, and number of total arm entries in IR-813 or PSNP-exposed mice. PSNPs exposure led to a decrease in the alternation rate, with no significant differences in total distance and arm entries across all groups. $*p < 0.05$ and $**p < 0.01$ compared to IR-813, one-way ANOVA.

(C) Radial arm maze test. Spectrum results of mouse movement (top) and quantification of total error ratio (bottom). A gradual decrease in error rate was observed for food location in the IR-813 treatment group during repeated trial sessions, while the error rate remained consistent in the PSNP-exposed group. $*p < 0.05$, $**p < 0.01$, and $***p < 0.001$ compared to IR-813 in each trial, two-way ANOVA.

(D) Barnes maze test. Tracking of mouse movement (top) and quantification of latency to target hole (bottom). A gradual decrease in escape latency was observed during the experimental session. PSNP exposure resulted in a persistence of error rates and increased latency to the target hole compared to IR-813 exposure. $*p < 0.05$ and $**p < 0.01$ compared to IR-813 in each day, two-way ANOVA.

(E) NORT results. PSNP exposure led to a reduction in the discrimination index. $*p < 0.05$ and $**p < 0.01$ compared to IR-813, one-way ANOVA.

(F) Light–dark transition test. All groups exhibited similar entry latencies during the training session. PSNP exposure resulted in reduced latency. $***p < 0.001$ compared to IR-813 in each day, two-way ANOVA.

(G) Step-down avoidance test. A gradual reduction in latency was observed during repeated trial sessions. PSNP exposure led to reduced latency compared to IR-813. $*p < 0.05$, $**p < 0.01$, and $***p < 0.001$ compared to IR-813 in each day, two-way ANOVA.

(H) Open field test. Measurement of locomotor activity by total distance and determination of anxiety behavior by the percentage of time spent in outer or central regions. All groups showed similar results in total distance and the ratio of time spent in outer *versus* central areas.

(I) Rotarod test. Similar latency to fall observed across all groups.

(J) Social behaviors using three-chamber tests. Top: Sociability test. Measurement of time spent in either the S1 or O chamber revealed significantly more time spent in S1 across all groups. $*p < 0.05$ compared to O, one-way ANOVA. Bottom: Social novelty test. Measurement of time spent in the S1 or S2 chamber showed significantly more time spent in S2 across all groups. $*p < 0.05$ compared to S1, one-way ANOVA.

(K) Organ distribution of PSNPs in mice following behavioral analyses. Representative images of IR-813 intensity in tissues from mice exposed to IR-813 or PSNPs using *in vivo* fluorescence imaging. Detection of IR-813 signals in the brain, stomach, intestines, liver, kidneys, and heart in PSNP-exposed mice but not in IR-813–exposed mice.

(L) Hippocampal sections from mouse brains exposed to IR-813 or PSNPs. Representative images of hippocampal sections stained with CD86. Magnified images corresponding to the dashed box.

arms for 10 min. Movements and arm entries were tracked using EthoVision software (Noldus, Wageningen, the Netherlands). Spontaneous alternation percentage was calculated by dividing the number of alternations (sequential entries into the three arms) by the total possible alternations (total arm entries minus 2), then multiplying by 100.

2.4.2. Radial arm maze test

Spatial working memory was evaluated using an eight-arm radial maze test. The apparatus included an octagonal central platform, 21 cm in diameter, with eight arms, each measuring 25 × 7 cm, surrounded by 7 cm high walls and elevated 80 cm from the floor. Mice were individually housed and food-restricted to maintain 80–90 % of their original body weight. During the training session, mice explored the maze for 15 min, with a food pellet placed in each arm. The session ended when all pellets were retrieved. For the test trial, four randomly chosen arms were baited with a pellet. Mice had 10 min to find the pellets, with the session ending after all pellets were retrieved or time elapsed. An overhead video camera (EthoVision XT, Noldus) recorded movements, and entry into a non-baited arm was recorded as an error.

2.4.3. Barnes maze test

Hippocampal-dependent spatial memory was evaluated using a

Barnes maze, an open circular platform 70 cm in diameter with 15 evenly spaced holes, each 5 cm in diameter. Spatial visual cues were placed on the room walls for the duration of the experiment. Mice underwent training twice daily, with at least a 30-min rest between trials. Each session began with the mouse on a central platform, encouraged to find a dark escape box (9 × 9 × 20 cm) beneath one of the holes. An overhead camera with EthoVision XT software tracked movements. Training lasted three days, followed by a probe test on the fourth day without the escape box. Trials ended when the mouse located the escape box or after 5 min. The maze was cleaned with 70 % alcohol after each trial to remove scent trails. Escape latencies to the target hole were recorded with EthoVision XT.

2.4.4. NORT

The NORT assessed hippocampal-dependent working memory. Mice were acclimated to the testing arena for 5 min. They then explored two identical objects placed equidistant from the center for 5 min. After 2 h, one object was replaced with a novel one of the same size but different shape. Mice explored both objects for another 5 min. Exploration time for each object was recorded, and a discrimination index was calculated as the percentage of time spent with the novel object.

2.4.5. Passive avoidance test

The light-dark transition test was conducted in an acrylic chamber (41 × 21 × 30 cm) with a non-illuminated compartment and an illuminated compartment lit by a 60 W bulb, connected by a guillotine door. The floor featured a stainless-steel grid for electrical shocks. During training, mice freely explored the illuminated chamber until they entered the dark compartment, triggering a door closure and a 0.3 mA shock for 3 s. Time spent in the illuminated chamber was noted. A 24-h follow-up test recorded the latency to enter the dark compartment, without shocks, up to 300 s. The step-down avoidance test used a chamber (21 × 20 × 20 cm) with a grid floor and a central platform (7 cm in diameter, 4 cm high). Mice received a 0.4 mA shock for 9 s upon stepping down during training. Follow-up tests at 24, 48, and 72 h measured step-down latency, without shocks, up to 300 s.

2.4.6. Open field test

The open field test assessed locomotor and anxiety behaviors. Mice were acclimated to a cage (42 × 42 × 40 cm) divided into inner and outer zones by EthoVision XT software. After 2 days of 30-minute habituation, mice explored the cage for 5 min. The total distance traveled and time spent in each zone were recorded by an overhead camera.

2.4.7. Rotarod

Locomotor activity was measured using a rotarod (B·S Technolab INC., Gyeonggi-do, Korea), accelerating from 4 to 40 rpm over 300 s. Mice underwent three trials per day with 5-minute rests, for three days. Latency to fall or reach 300 s was recorded, with the average latency noted for each mouse.

2.4.8. Three-chamber test

Sociability and social novelty were assessed using the three-chamber test, as described by Kim et al. (2022). The apparatus comprised three interconnected rectangular chambers, each measuring 21 × 23 × 42 cm. During the habituation phase, the subject mouse was placed in the central chamber and allowed to explore the adjacent chambers, each containing a round wire cup, for 10 min. In the sociability phase, a stranger mouse (S1) was placed in one wire cup, while the other cup remained empty (O). The subject mouse's movements were recorded for 10 min. In the social novelty phase, a novel mouse was introduced into the previously empty cup. The subject mouse was then allowed to explore for an additional 10 min, with the time spent in each compartment recorded by EthoVision XT.

2.5. Immunohistochemistry

Following behavioral analyses, mouse brains were dissected and fixed in 4 % neutral-buffered paraformaldehyde for 12 h. Tissues were embedded in paraffin and sectioned at 5 μm, including the hippocampus. Sections were deparaffinized and incubated with primary antibodies against CD86 (1:100, Abcam) in a blocking buffer of 5 % donkey serum and 0.3 % Triton X-100 in DPBS overnight at 4 °C. After three washes, sections were stained with Alexa488-conjugated secondary antibody (1:200, Abcam) for 1 h at 15–25 °C in a light-protected chamber. Slides were mounted with DAPI-containing mounting media (Vector Laboratories) and imaged with a confocal microscope (LSM 800, Zeiss).

2.6. Primary cultures and treatment

Primary cultures of microglia and astrocytes were established with minor modifications to the methods described by Vay et al. (2018). Cerebral cortices from 1-day-old Sprague-Dawley rat pups (Young Bio, Gyeonggi-do, Korea) were mechanically dissociated through pipetting and filtered through a 70-μm cell strainer (BD Biosciences, NJ, USA). The resulting cell suspensions were cultured in Dulbecco's Modified Eagle's Medium/Nutrient Mixture F12 (DMEM/F12, Thermo Fisher Scientific, MA, USA), supplemented with 10 % fetal bovine serum (FBS, Youngin, Gyeonggi-do, Korea), 100 μg/mL streptomycin, and 100 U/mL penicillin, and maintained at 37 °C in a 5 % CO_2 humidified environment for seven days. Microglia were isolated from confluent co-cultures by agitation at 250 rpm for 1 h at 37 °C on an orbital shaker. The detached microglia were collected by centrifugation for 2 min at 1200 rpm. After removing the supernatant, microglia were cultured in DMEM/F12 with 10 % FBS and 1 % penicillin-streptomycin, then seeded onto poly-D-lysine (PDL, Merck, NJ, USA)-coated plates for 3 more days. Astrocytes were enzymatically detached from confluent co-cultures using 0.25 % trypsin and EDTA (ethylenediaminetetraacetic acid), then seeded onto PDL-coated plates and cultured for an additional 5 days in DMEM/F12 with 10 % FBS and 1 % penicillin-streptomycin.

Primary hippocampal neuron cultures were prepared following the protocol of Wu et al. (2016). Hippocampi from P1 rat pup brains were dissociated into single cells using trypsin. Neurons were resuspended in Neurobasal medium containing 1 % GlutaMAX (Thermo Fisher Scientific), 2 % B27 (Thermo Fisher Scientific), and 1 % penicillin/streptomycin, then seeded onto PDL-coated plates and cultured in a humidified incubator at 37 °C and 5 % CO_2 for further analysis.

Cultured cells were treated with IR-813 (200 μg/mL) or PSNPs (200 μg/mL) for 24 h to assess PSNPs internalization. Microglia were incubated with IR-813 (500 μg/mL) or PSNPs (200 or 500 μg/mL) for 24 h to examine microglial activation. To explore whether neuroinflammation influences PSNPs uptake, microglia were treated with DPBS or lipopolysaccharide (LPS, 10 ng/mL, Merck) for 2 h, then incubated with PSNPs (200 μg/mL) for 24 h. RNA sequencing (RNA-seq) analysis and transcript levels were evaluated in microglia treated with IR-813 (200 μg/mL) or PSNPs (200 μg/mL) for 24 h.

2.7. Immunocytochemistry and three-dimensional scanning

Coverslips were rinsed three times with DPBS and fixed with 4 % paraformaldehyde for 15 min at 15–25 °C. They were then permeabilized in a 0.1 % Triton X-100 solution for 10 min. Cells were probed with primary antibodies against IBA1 (1:200, Thermo Fisher Scientific), glial fibrillary acidic protein (GFAP, 1:400, Abcam), MAP2 (1:400, Santa Cruz Biotechnology, CA, USA), CD86 (1:200, Abcam), and p65 (1:400, BD Biosciences) in a blocking buffer of 1 % bovine serum albumin in DPBS overnight at 4 °C. After three washes, coverslips were incubated with Alexa488 or Alexa594-conjugated secondary antibodies (1:200, Abcam) for 1 h at 15–25 °C in a light-protected chamber. Nuclei were stained with a 0.5 μg/mL DAPI solution (Thermo Fisher Scientific).

The coverslips were mounted with gel mount solution (Biomeda, CA, USA) and imaged with a confocal microscope (Zeiss). Lateral cellular images were captured using a 60× oil objective lens with the z-stack function, creating stacks of 70 × 70 × 5 μm with 0.3 μm-thick sections. Three-dimensional reconstructions were generated with Zen software (Zeiss), and the internalization of PSNPs within cellular markers was quantified.

2.8. RNA-seq analysis

Total RNA was isolated from rat primary cells using the Direct-Zol™ RNA Microprep Kit (Zymo Research, CA, USA), following the manufacturer's protocol. Genomic DNA contamination was removed with a 15-min on-column DNase I treatment at room temperature. RNA quantification was performed using the PicoGreen Assay (Thermo Fisher Scientific), and RNA quality was evaluated with the RNA ScreenTape on the 4200 Tapestation system (Agilent Technologies, CA, USA). We enriched 1000 ng of total RNA for mRNA using the NEBNext Poly(A) mRNA Magnetic Isolation Module (New England BioLabs, MA, USA). Fragmentation, cDNA synthesis, and library preparation with unique dual indexing were conducted using the NEBNext Ultra II RNA Library Prep Kit (New England BioLabs), according to the manufacturer's instructions. The libraries were sequenced on the NovaSeq 6000 platform (Illumina, CA, USA) with 100 bp paired-end reads. Three RNA samples per group were analyzed. Data analysis was conducted using the ExDEGA program (ebiogen, Seoul, Korea) to create volcano plots, showing the relationship between fold change values and −log10 (*p*-value) for differentially expressed genes. Principal component analysis (PCA) was performed with the ExDEGA Graphic Plus program to obtain PCA scores and variance percentages. Functional gene-annotation enrichment analysis was conducted using the DAVID tool (National Institutes of Health, MD, USA), with visualization through the ExDEGA Graphic Plus program. Sample and gene clustering were performed using MeV version 4.9.0, with hierarchical cluster analyses based on Euclidean distance correlation and average linkage methods. Clusters and heat maps were generated using MeV 4.9.0.

2.9. Quantitative real-time polymerase chain reaction (qRT-PCR)

Total RNA was extracted from cultured rat primary cells using TRIzol reagent. First-strand cDNA synthesis was performed using MultiScribe Reverse Transcriptase and random primers. The qRT-PCR assays were conducted using Power SYBR Green PCR Master Mix (Thermo Fisher Scientific). Primer sequences for these assays are listed in Table 1. Glyceraldehyde 3-phosphate dehydrogenase (GAPDH) was used as the internal control for normalization. Relative mRNA quantification was determined using the geometric mean of the cycle threshold (Ct) values of the internal control, obtained with the QuantStudio 1 Real-Time PCR System (Thermo Fisher Scientific).

2.10. Collection of conditioned medium (CM) from microglia

For CM collection, 8×10^5 microglial cells were seeded and subsequently subjected to a medium exchange with 1 mL of fresh medium. This medium was harvested after an additional 24-hour incubation with either IR-813 (200 μg/mL) or PSNPs (200 μg/mL). Disease-associated microglia (DAM) inhibitors, AMY-101 TFA (C3 inhibitor, 10 μM, MedChemExpress, NJ, USA) and ZINC00640089 (Lcn2 inhibitor, 10 μM, MedChemExpress), were administered to microglia 2 h prior to PSNP application. The collected CM was filtered through a 0.2 μm pore size filter using Whatman Puradisc 25 syringe filters (Merck) to remove debris, aggregates, or particles, and was immediately applied to hippocampal neurons.

Table 1
Primer list.

Name	Forward	Reverse
C3	AGGGTGGAACTGTTGCATAACC	TGGTCTGGTAGTACCGCTTCTTG
Lcn2	GGGCAGGTGGTTCGTTGTC	AGCGGCTTTGTCTTTCTTTCTG
Myd88	CCTTGCAGGTGGCCAGAGT	TGATGCCTCCCAGTTCCTTT
Spp1	CGGCCTTGCCTCCTGTCT	TCTCCTCTGAGCTGCCAAACTC
Cd9	CGGACATCTGCCCCAAAA	TCCGGGCAGGACTTAACCT
Lpl	AACCCCAGCAAGGCATACAG	AGGCAGAGCCCTTTCTCAAAT
Gapdh	CCTGGAGAAACCTGCCAAGTAT	CTCGGCCGCCTGCTT

2.11. Multi-electrode array (MEA)

Spontaneous neuronal activity in cultured hippocampal neurons was assessed using an MEA system consisting of 24 individual wells (M384-tMEA-24 W, Maestro Systems, Axion Biosystems, GA, USA). The electrodes, made of poly(3,4-ethylenedioxythiophene), had a diameter of 50 μm and were spaced 350 μm apart. Neurons were plated at a density of approximately 550–600 cells per mm^2 onto MEA dishes (total 1×10^5 cells/well). Each MEA plate featured 16 electrodes arranged in a 4 × 4 grid within a transparent well of 15 mm diameter. Recordings were made on *in vitro* day 14 after a 15-min stabilization period, acquiring data for 15 min at a sampling rate of 12.5 kHz with a band-pass filter between 200 and 3000 Hz. Experiments were conducted at 37 °C with 5 % CO_2. Data analysis was performed using AxIS software (ver. 3.6.2, Axion Biosystems) to identify bursts (≥5 spikes with an inter-spike interval (ISI) of <100 ms) and network bursts (≥25 spikes with an ISI of <50 ms).

2.12. Statistical analysis

Data are presented as mean ± standard error of the mean. Statistical analyses were performed using GraphPad Prism 5 (GraphPad Software, Inc., Boston, MA, USA). The Mann-Whitney *U* test was used for non-normally distributed datasets, and one-way ANOVA followed by Tukey's *post hoc* test or two-way ANOVA followed by Bonferroni's *post hoc* test was employed for interaction groups. Cellular experiments were replicated in at least three independent cultures.

3. Results

3.1. Synthesis and characterization of PSNPs

Considering the widespread use of spherical micro- and nanoplastics in previous studies to explore the neurotoxicity of plastics (Nikolic et al., 2022; Prust et al., 2020), we initially synthesized spherical nanoplastics without fluorescence (pristine) as depicted in Fig. 1A. We also synthesized pristine nanoplastics incorporating the IR-813 fluorophore, which possesses extended wavelength properties enabling deeper penetration into target organs. Additionally, to prevent artifacts from fluorescent leaching, IR-813 was embedded within the pristine nanoplastics. The synthesized pristine and PSNPs underwent validation through multiple methods. Firstly, the fluorescence of both pristine and PSNPs was confirmed using a fluorescence *in vivo* imaging system, with PSNPs exhibiting significantly stronger fluorescence emission around 813 nm compared to the pristine (Fig. 1B). Secondly, SEM verified the spherical morphology and size of both pristine and PSNPs (Fig. 1C). Thirdly, DLS analysis indicated a size distribution between 30 and 50 nm (Fig. 1D). Lastly, the compositional integrity of both pristine and PSNPs was affirmed by Fourier-transform infrared (FTIR) spectroscopy (Fig. 1E). For the IR spectrum acquisition, a small quantity of polymer powder was placed on the attenuated total reflectance crystal, pressure was applied, and then FTIR analysis was conducted. These results confirmed the size and shape of the nanoplastics, which were subsequently utilized for further *in vivo* and *in vitro* analyses.

3.2. Cognitive dysfunction by oral ingestion of PSNPs in mice

To investigate the neurotoxic effects of PSNPs, mice received oral doses of PSNPs (10 and 20 mg/kg), and behavioral tests were conducted as outlined in Fig. 2A. IR-813 (20 mg/kg/mice) served as a control. Mice were treated daily with IR-813 or PSNPs for 7 weeks and sacrificed in the 8th week for additional analyses. Behavioral analyses assessed cognitive function, locomotor activity, anxiety, and social behaviors. Spatial cognitive memory was evaluated using Y-maze, radial arm maze, and Barnes maze tests, while cognitive function was measured by the NORT. Considering the impact of acute stress on cognitive performance (Sandi, 2013), fear memory was assessed later in the exposure period using light-dark transition and step-down avoidance tests, with a 1-week resting interval. In the Y-maze test, PSNPs-exposed mice showed a lower alternation rate than those exposed to IR-813, with total distance and arm entries remaining similar (Fig. 2B). Radial arm maze tests revealed that IR-813-exposed mice progressively reduced total errors across trials, whereas PSNPs-exposed mice maintained consistent error levels and had a significantly higher error rate compared to the vehicle (Veh) group (Fig. 2C). In the Barnes maze test, both IR-813 and PSNPs-exposed mice gradually decreased latency to locate the target hole, but PSNPs-exposed mice had longer latencies (Fig. 2D), suggesting impaired spatial working memory. Additionally, PSNPs-exposed mice showed reduced discriminatory ability in the NORT (Fig. 2E). Fear-related cognitive assessments using passive avoidance tests indicated that, during the light-dark test, latency to enter the dark compartment was similar across all groups during training; however, PSNPs exposure resulted in reduced entry latency (Fig. 2F). The step-down avoidance test also showed that PSNPs-exposed mice had shorter latency times compared to the Veh group (Fig. 2G). These findings collectively suggest that PSNPs exposure adversely affects learning and memory functions in mice.

We also investigated the influence of PSNPs on mice's locomotor activity and anxiety behavior. Open field test results revealed no significant differences in the total distance traveled by PSNPs-exposed mice, indicating that PSNPs exposure does not affect locomotor behavior or induce anxiety-like behavior (Fig. 2H). Similarly, the rotarod test confirmed that locomotor activity, as measured by latency, was unaffected by PSNPs exposure compared to IR-813 exposure (Fig. 2I). The influence of PSNPs on sociability and social novelty was evaluated using a three-chamber test. Initially, both IR-813 and PSNPs-exposed mice showed a preference for the subject chamber over the object chamber (Fig. 2J). In subsequent tests with familiar (S1) and stranger (S2) mice, PSNPs-exposed mice spent more time with the stranger mice, consistent with the behavior of IR-813-exposed mice, indicating no significant changes in social behaviors due to PSNPs exposure.

To investigate whether orally administered PSNPs reach the brain, we assessed the distribution of PSNPs in mouse organs using a fluorescence *in vivo* imaging system for post-behavioral analyses. PSNPs were predominantly found in the stomach, intestine, liver, and kidney, with notable accumulation also observed in the brain (Fig. 2K), suggesting that the synthesized PSNPs can cross into brain tissues. Additionally, increased expression of CD86, a marker for activated microglia, was observed in the hippocampus following PSNPs exposure (Fig. 2L). These findings imply that chronic oral ingestion of nanoplastics leads to microglial activation, potentially contributing to the observed cognitive dysfunctions in mice.

3.3. Internalization of PSNPs in microglia

Understanding the cellular internalization of plastics is pivotal for elucidating the underlying toxic mechanisms in living organisms. To this end, we investigated the cellular uptake of PSNPs in different types of brain cells. Primary cultures of microglia, astrocytes, and neurons were exposed to either IR-813 or PSNPs and subsequently immunostained with cell-specific markers: IBA1 for microglia, GFAP for astrocytes, and MAP2 for neurons. The cells were imaged using both two- and three-dimensional scanning techniques to assess the cellular uptake of PSNPs. Top-view imaging revealed PSNP signals on microglial cells, and side-view imaging displayed internalized PSNPs in microglia, as evidenced by PSNP fluorescence signals located beneath the IBA1 staining (Fig. 3A, arrowhead). Additionally, the morphology of microglial cells was altered upon PSNP uptake. Interestingly, although top-view imaging indicated the presence of PSNP signals on astrocytes and neurons, PSNP signals were observed above the GFAP or MAP2 staining in side-view images (Fig. 3B and C, arrow), indicating that PSNPs were not internalized in these cells. Hence, our results suggest that PSNPs adhere to the cellular membranes of astrocytes and neurons but are not internalized. Quantitative analysis of the proportion of cells displaying PSNP uptake and the intensity of internalized PSNPs revealed that microglial cells predominantly internalized PSNPs (Fig. 3D), consistent with the findings of a previous study (Murali et al., 2015).

3.4. PSNP uptake induces microglial activation and neuroinflammation

Given that the immune response of microglia triggers their transformation from a ramified to an activated, and eventually, amoeboid form (Colonna and Butovsky, 2017; Leyh et al., 2021), we further investigated whether the uptake of PSNPs leads to microglial activation. In the presence of IR-813, resting ramified microglia were observed, whereas microglia that internalized PSNPs displayed an amoeboid phagocyte form (Fig. 4A). Moreover, an enlarged cell area in microglia that had internalized PSNPs indicated microglial activation (Edler et al., 2021). We also found that the expression of CD86 was increased by PSNP exposure (Fig. 4B). P65:p50 is the most abundant form of NF-κB, which is a critical transcription factor associated with inflammatory responses (Giridharan and Srinivasan, 2018). In resting conditions, p65:p50 dimers are kept inactive by interacting with the inhibitory protein IκB. The activation of NF-κB induces degradation of IκB, which in turn releases p65:p50 and induces nuclear translocation and transcriptional activity (Oeckinghaus and Ghosh, 2009). PSNP exposure enhanced the nuclear translocation of p65 (Fig. 4C). To further explore whether neuroinflammation aggravates nanoplastic uptake in microglia, PSNPs were applied to LPS-stimulated microglia. We found that exposure to LPS increased PSNP uptake by microglia (Fig. 4D). These results indicate that PSNP uptake by microglia not only leads to microglial activation and neuroinflammation but also further enhances the uptake of PSNPs in microglia.

3.5. PSNPs induce transcriptional changes in RNA-seq analysis

To elucidate the mechanisms behind cognitive impairment caused by PSNPs, RNA-seq analysis was conducted on microglia treated with IR-813 (200 μg/mL) or PSNPs (200 μg/mL). After read alignment and quantification, we performed PCA using 16,876 highly expressed transcripts to discern variations between samples from rat primary cells treated with IR-813 alone and those with PSNPs (Fig. 5A). The first two principal components accounted for the most variance in the RNA-seq data. DESeq2 analysis identified 4546 differentially expressed transcripts (DETs) in PSNPs-treated samples (Fig. 5B). Volcano plots visualized the statistical significance and fold changes of DETs ($p < 0.01$, absolute log2 fold-change [log2 FC] > 1) compared to controls. Notably, 2131 transcripts were upregulated, while 2415 were downregulated in PSNPs-treated microglia. Hierarchical clustering was applied to 1156 upregulated and 1363 downregulated transcripts under stringent conditions ($p < 0.01$, log2 FC > 1.5) (Fig. 5C). Top enriched gene ontology (GO) categories in cellular components and biological processes were visualized for cells exposed to PSNPs (Fig. 5D and E). GO analysis showed that inflammatory response-related transcripts were significantly affected by PSNPs. qRT-PCR validated increased expression of inflammation-related genes such as complement C3, lipocalin 2 (Lcn2),

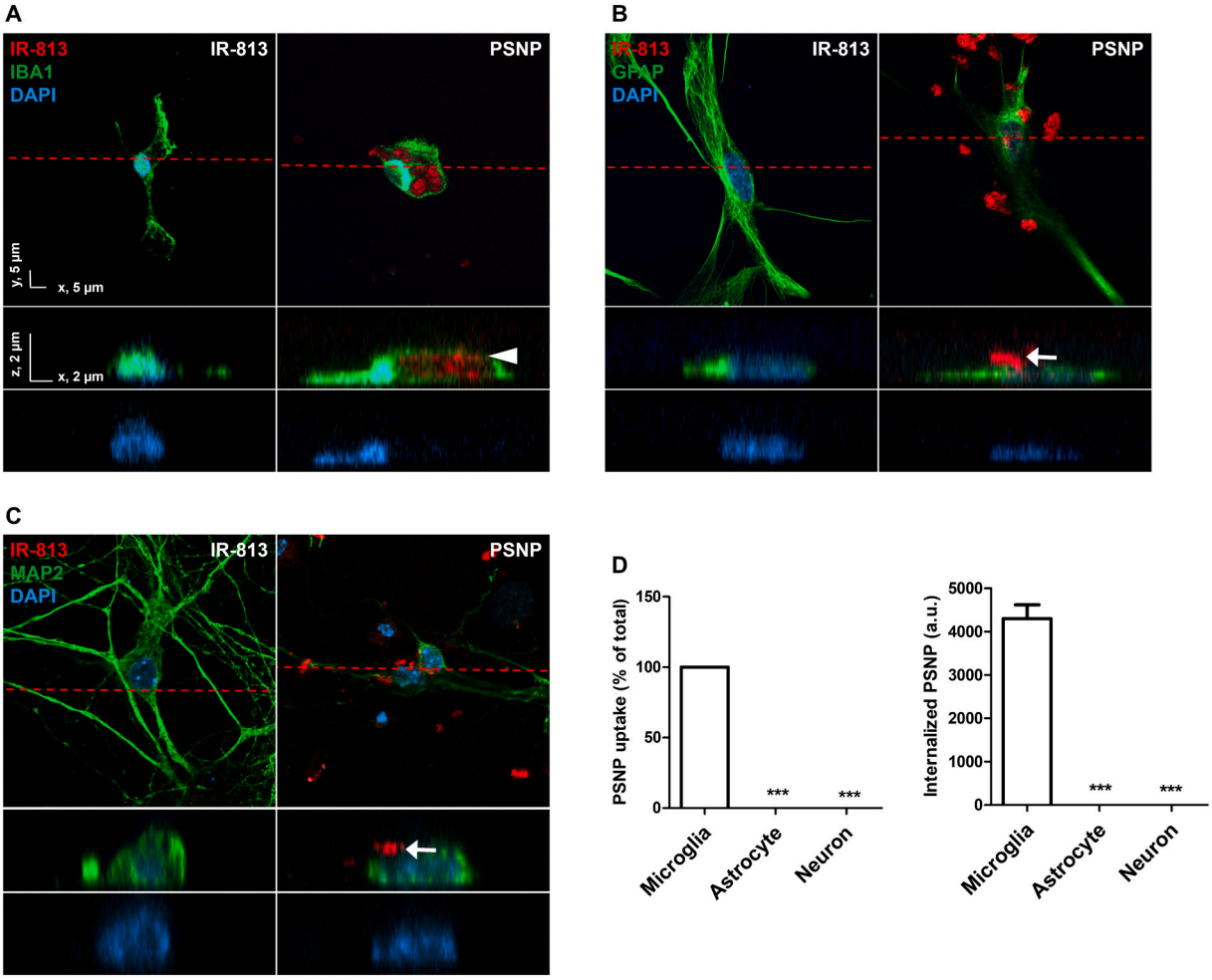

Fig. 3. Internalization of PSNPs in microglia.
Primary cultured microglia, astrocytes, and neurons were incubated with either IR-813 (200 µg/mL) or PSNPs (200 µg/mL) for 24 h and stained with IBA1, GFAP, and MAP2, respectively.
(A-C) Top: Representative top view images of microglia (A), astrocytes (B), and neurons (C). Middle: Magnified side views corresponding to the dashed red lines in the three cell types. Indication of internalized PSNPs (arrowhead) or attached PSNPs on the cellular surface (arrow). Bottom: Visualization of changes in nuclear morphology by DAPI staining.
(D) Quantification of the cellular ratio of PSNPs uptake (left) and internalized PSNPs intensity within the cells (right). ***$p < 0.001$ compared to microglia; analyzed using the Mann-Whitney *U* test.

and Myd88 following PSNP treatment (Fig. 5F). Additionally, mRNA expression of DAM genes like secreted phosphoprotein 1 (Spp1), tetraspanin 9 (Cd9), and lipoprotein lipase (Lpl) was enhanced by PSNPs. These findings suggest that PSNPs activate inflammatory responses and phagocytic activities, potentially worsening neurodegenerative conditions in microglia.

3.6. Blockade of C3 and Lcn2 restores the neuronal function impaired by PSNP exposure

To determine the mechanisms behind the learning and memory deficits induced by PSNPs, we evaluated the spontaneous activity and network function of cultured hippocampal neurons using MEA in the presence of CM. The CM, collected from microglia exposed to IR-813 or PSNPs, was filtered to eliminate cells, debris, and particles (Fig. 6A). Neuronal activity, measured by MEA post-CM application, was similar between the Veh group (treated with neuron culture medium with the same volume of CM from IR-813) and neurons treated with CM from IR-813. However, CM from PSNPs reduced neuronal activity, notably in firing rate, burst rate, and network bursts (Fig. 6B). To confirm that soluble factors from activated microglia mediate neuronal suppression, microglia were pre-treated with C3 or Lcn2 inhibitors before PSNPs exposure. CM from these treated microglia, when applied to neurons, mitigated the neuronal suppression caused by PSNPs. Although CM from PSNPs decreased burst firing rate, the ISI within bursts was consistent across groups. These findings suggest that microglia activated by PSNPs release soluble factors that suppress hippocampal neuronal activity, potentially leading to cognitive dysfunction in mice.

4. Discussion

Emerging evidence indicates the presence of nanoplastics in the environment, but their impact on human health and the natural environment remains largely unquantified or unknown (Chae and An, 2017). It is crucial to acknowledge that the doses of PSNPs used in our study, both *in vitro* and *in vivo*, are relatively higher than those typically encountered in the environment, aligning our research more with hazard characterization than direct risk assessment. However, recent studies are increasingly reporting higher concentrations of microplastics in the human body compared to their presence in the environment. For instance, a recent study estimated that the accumulation of microplastics in the human lungs and intestines could be as high as 46 mg and

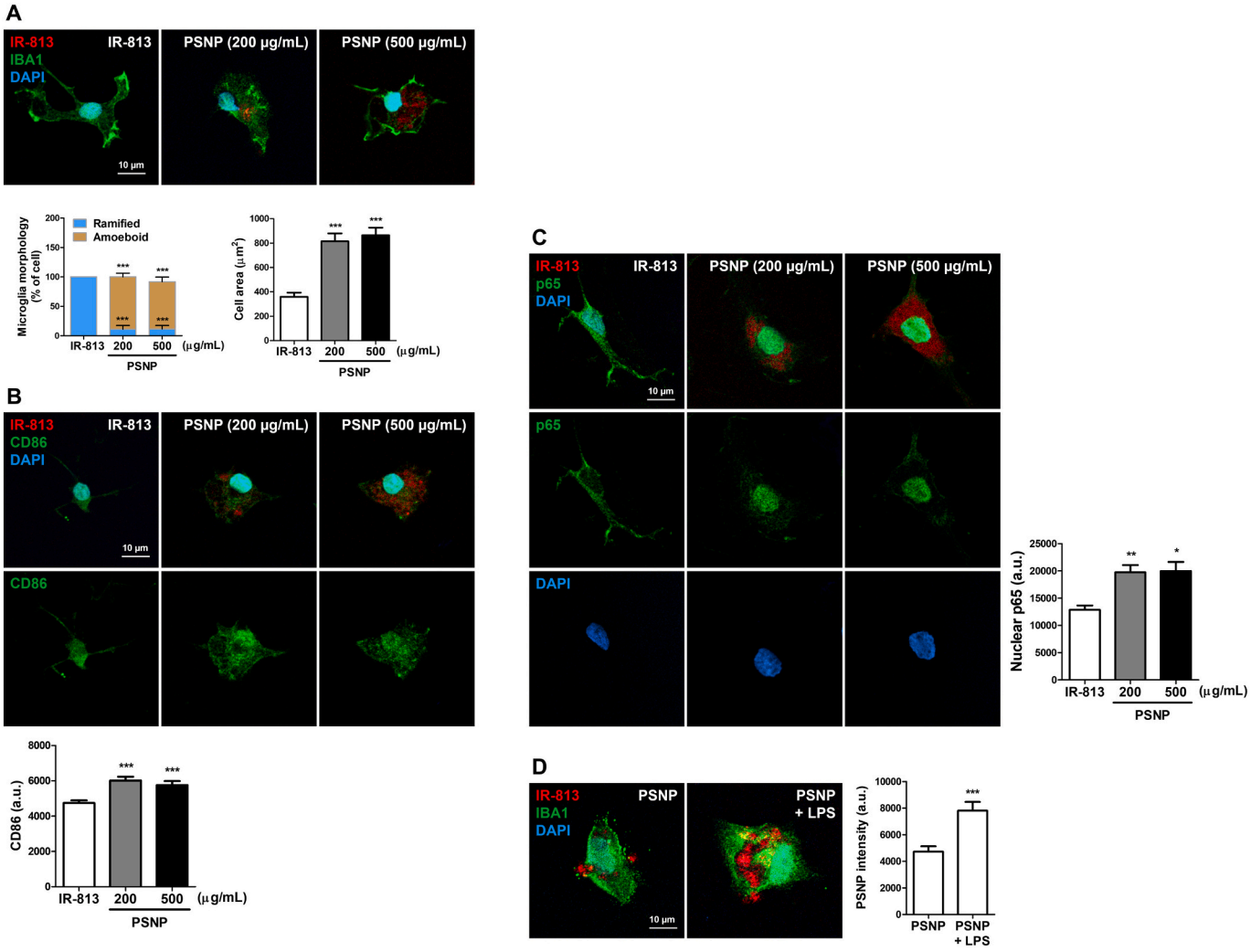

Fig. 4. Internalization of PSNPs induces microglial activation.
(A) Incubation of primary cultured microglia with IR-813 (500 μg/mL) or PSNPs (200 or 500 μg/mL) for 24 h and subsequent staining with IBA1. Representative images (top) and quantification (bottom, left) show the cellular proportions of ramified and amoeboid microglia. Quantification of cell area by IBA1 positive signals (bottom, right). Using two-way ANOVA and one-way ANOVA for analyzing morphological analysis and cell area, respectively. ***$p < 0.001$ compared to IR-813.
(B) Same as (A) but with CD86 staining. Representative images and quantification results showed elevation of CD86 expression by PSNP exposure in microglia. ***$p < 0.001$ compared to IR-813, one-way ANOVA.
(C) Same as (A) but with p65 staining. Staining of nuclei with DAPI. Representative images and quantitative analysis indicated translocation of p65 into the nucleus in microglia exposed to PSNPs. *$p < 0.05$ and **$p < 0.01$ compared to IR-813; one-way ANOVA.
(D) Neuroinflammation increased PSNP uptake in microglia. Microglia were treated with DPBS or LPS (10 ng/mL) and subsequently incubated with PSNPs (200 μg/mL). Representative images and quantification of PSNP intensity in microglia. ***$p < 0.001$ compared to PSNP; analyzed using the Mann-Whitney U test.

4.71 mg, respectively (Zhu et al., 2024). Another significant finding revealed the presence of microplastics in the human placenta, measured at approximately 126.8 μg/g (Garcia et al., 2024). It is important to note, however, that while many studies have focused on microplastics, nanoplastics have received less attention, likely due to the challenges in detecting smaller particles.

The ability of nanoparticles to penetrate the blood-brain barrier (Kim et al., 2006; Meyers et al., 2013) or access the brain *via* the nasal epithelium (Mistry et al., 2009) raises serious concerns about their potential neurotoxicity (Chen et al., 2017). While fragments, aggregates, or fibers are considered common forms of plastics in the environment, the wide size range and diverse morphology of plastics challenge the quantitative analysis of nanoplastics and environmental risk assessment. Spherical nanoplastic particles, either manufactured as primary particles or produced by grinding microplastics, are significant sources of plastic contaminants (Hwang et al., 2020). These spherical microplastics or nanoplastics are commonly used to study the toxic effects of plastics on human health and biological systems. The detection of spherical or granular shapes in smaller plastic particles, unlike the irregular forms found in larger aggregates (Monikh et al., 2023), together with the identification of spherical nanoplastics in real-world samples (Peller et al., 2022), underscores their environmental significance. A recent study revealing that 90 % of plastics in bottled mineral water consist of spherical nanoplastics (Qian et al., 2024) indicates that exposure to spherical nanoplastics from processed sources might be higher than previously estimated from environmental nanoplastic concentrations (Materic et al., 2022). Therefore, while the spherical nanoplastics used in our experiments may not fully encompass the diverse morphologies of environmental plastics, they present a focused perspective that aligns with emerging evidence of nanoplastic accumulation in the human body and provide broader implications for understanding human exposure to nanoplastics and their potential health impacts.

In this study, we explored the neurotoxic effects of PSNPs on adult mouse behavior and their internalization in primary neural cells.

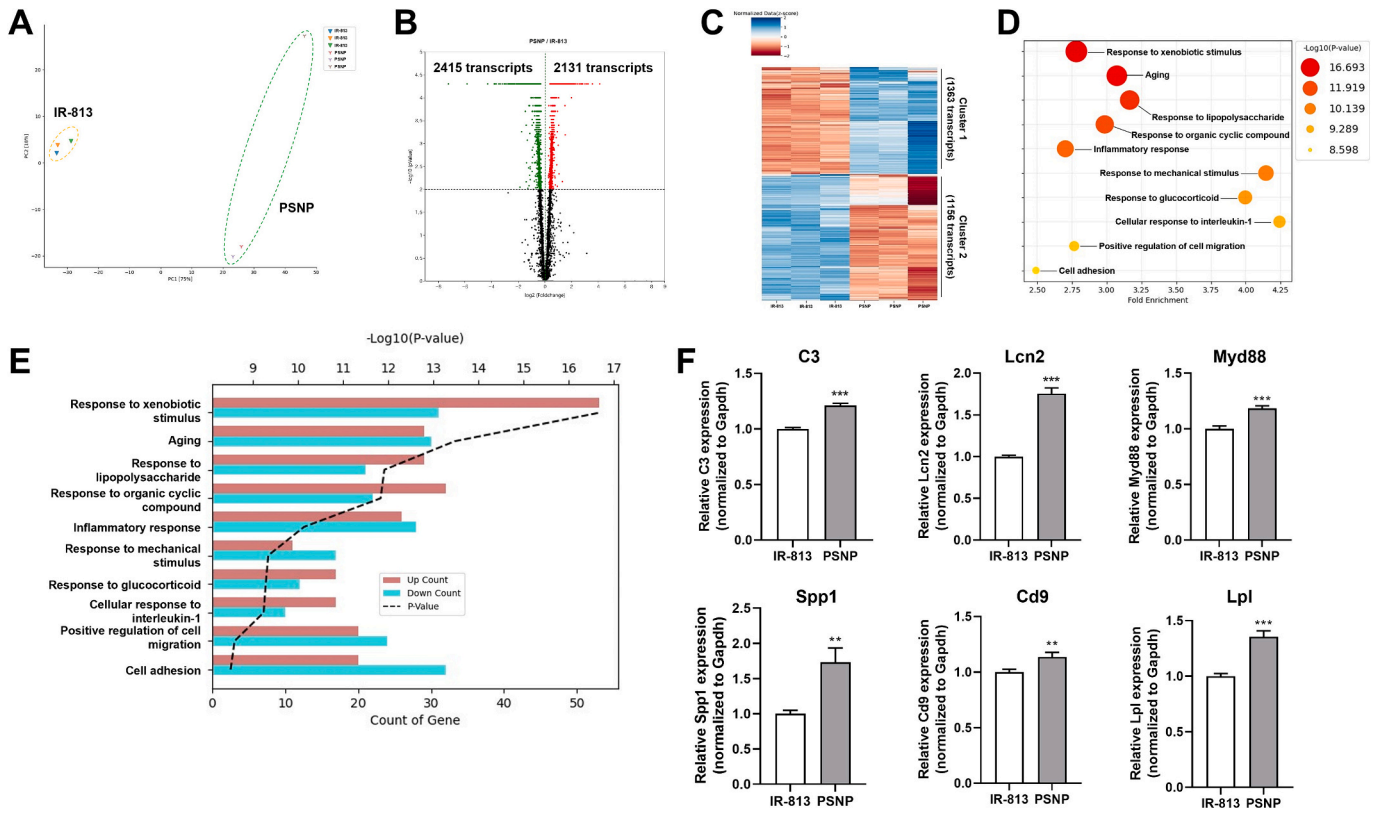

Fig. 5. Changes in mRNA expression in microglia following PSNPs exposure.

(A) PCA of RNA-seq data illustrating the variance in gene expression profiles. The PCA plot clarifies the proportion of variation attributable to each principal component in the data set, with individual samples distinctly marked for IR-813 (▼) and PSNPs (Y) treatments.

(B) A volcano plot visually highlights significant differentially expressed transcripts (DETs) in microglia after PSNP treatment compared to the IR-813 control, emphasizing genes with significant upregulation or downregulation.

(C) Hierarchical clustering analysis of differential gene expression patterns, presented in a matrix format with rows representing individual genes and columns corresponding to experimental samples. This clustering is based on RNA-seq data, with criteria for differential expression including fold change values >1.5 and a significance level of $p < 0.01$.

(D) A plot visualizes the enriched GO cellular components and biological processes in PSNP-treated microglia, using significantly upregulated DETs from RNA-seq data, with circle sizes indicating the number of genes in each category and color intensity reflecting significance levels (−log10 of the *p*-value).

(E) The top 10 functional categories from DAVID GO chart analysis are presented, showing the number of genes in each category for both upregulated and downregulated genes. Significantly enriched terms ($p < 0.01$) from differentially expressed transcripts are displayed in descending order of significance (−log10 of *p*-value) and gene count.

(F) Quantitative qRT-PCR analysis of key gene transcripts (C3, Lcn2, Myd88, Spp1, Cd9, and Lpl) in microglia. *$p < 0.05$, **$p < 0.01$, and ***$p < 0.001$ compared to IR-813, analyzed using the Mann-Whitney U test.

Considering that the brain toxicity of nanoplastics has been less studied than other organs (Ramsperger et al., 2020), our findings provide valuable insights into the toxic mechanisms of PSNPs in neural tissues. Although oral ingestion of nanoplastics is known to impair brain functions, distinguishing between direct effects on the brain and secondary effects from other tissues, such as immune activation in the intestine (Yang et al., 2023), is challenging. Observing particle deposition within tissues can help determine whether the effects of nanoplastics are direct or indirect (Xu et al., 2020). In our study, the accumulation of fluorescence signals from PSNPs may indicate a direct impact of nanoplastics on brain toxicity following oral exposure.

The assessment of plastic toxicity is influenced by various experimental variables. For example, increased temperature has been shown to enhance plastic-induced toxicity in fish, resulting in elevated acetylcholinesterase (AChE) levels and lipid peroxidation (Fonte et al., 2016). The surface charge of plastic particles also affects cellular toxicity (Roshanzadeh et al., 2020). Given that plastics rapidly adsorb lipids and proteins upon exposure (Galloway et al., 2017; Rummel et al., 2017), it is plausible that surface charge characteristics play a role in the interaction between plastics and biomolecules, thus affecting toxicity. Additionally, sonication of plastics can alter their toxicological profile (Vaz et al., 2021). Finally, the size of plastic particles is another critical factor that influences their toxicity potential (Schroter and Ventura, 2022). Therefore, providing detailed information about the types of plastics used and the exposure conditions in experiments is essential for accurate risk assessment of plastic exposure in humans. Using conjugated dyes or fluorescence for plastic labeling as a control may help minimize experimental artifacts. Our findings indicate that mice treated with IR-813 exhibited similar cognitive and locomotor activity compared to those treated with normal saline (Supplementary Fig. 1). Furthermore, oral ingestion of pristine resulted in cognitive dysfunction but normal locomotor activity in mice (Supplementary Fig. 2), paralleling PSNPs exposure. This supports the conclusion that cognitive impairment from PSNPs exposure is mediated by nanoplastics rather than dye. The varying periods of PSNPs exposure (2–7 weeks) for total behavioral analyses present a concern in this study. We observed that cognitive function impairment, but not locomotor activity, caused by PSNPs was reproducible with one week and five weeks of exposure (data not shown), confirming that PSNPs exposure affects multiple memory types, including short-term and long-term memory. Another point of consideration is the investigation of neurotoxic effects of PSNPs in two rodent models: *in vivo* in mice and *in vitro* in rats. As the evaluation of

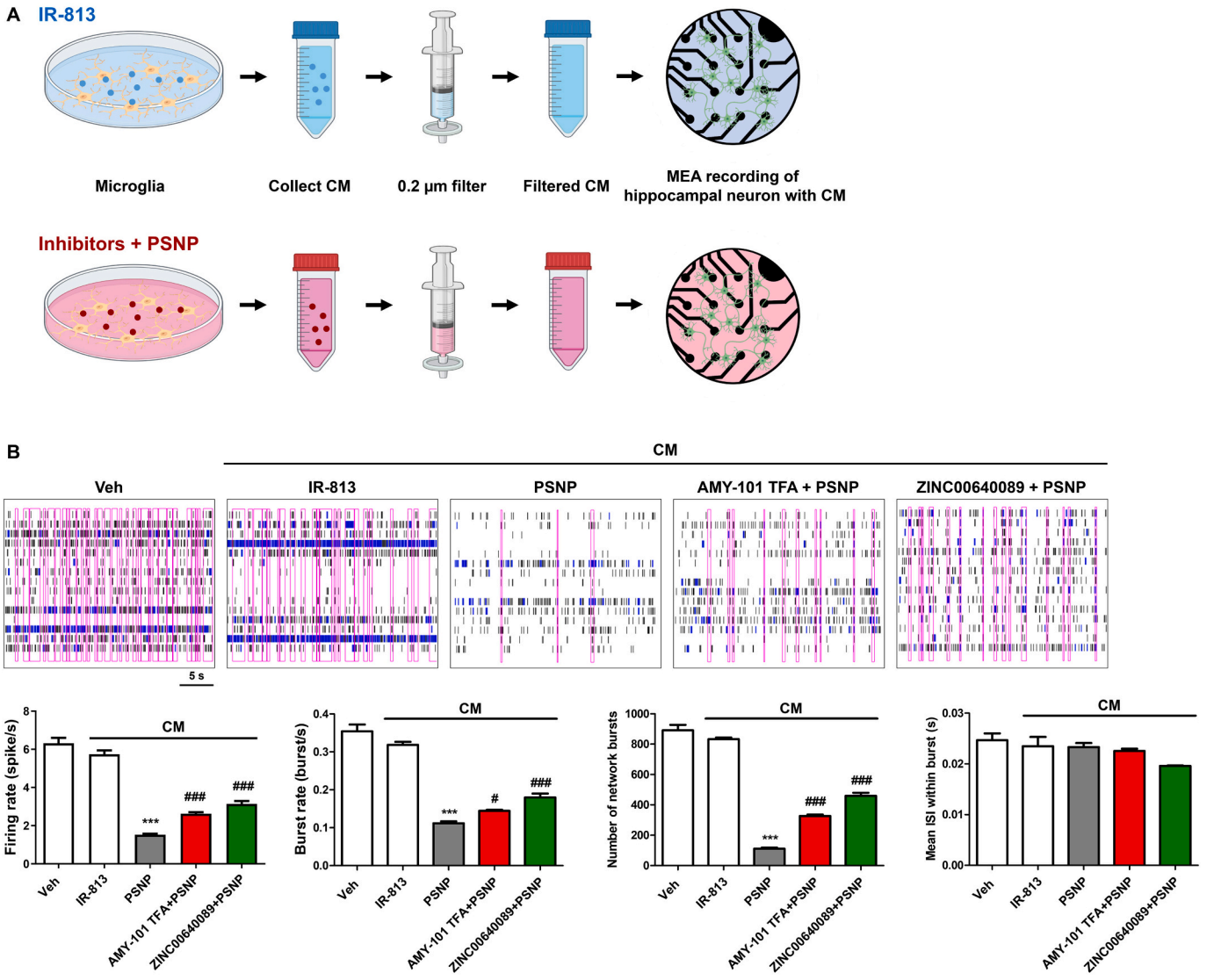

Fig. 6. Inhibition of C3 or Lcn2 alleviates neuronal suppression induced by the application of CM from PSNP-exposed microglia.
(A) Experimental design for measuring neural activity following CM application. CM was collected from microglia incubated with either IR-813 (200 μg/mL, blue) or PSNPs (200 μg/mL, red) with or without inhibitor for 24 h. Inhibitors of C3 or Lcn2 were treated to microglia before 2 h of PSNP application. The filtered CM was applied to mature hippocampal neurons (green) seeded on MEA plates, and then spontaneous neuronal activity was measured.
(B) Top: Spike train data from 16 MEA electrodes, following the application of CM from microglia exposed to IR-813 or PSNPs with or without C3 or Lcn2 inhibitor. Veh refers to the application of neuronal culture medium with same volume of IR-813. Indication of individual firing spike (black), burst firing (blue), and network bursts (pink). Bottom: Quantification of firing rate, burst rate, number of network bursts, and ISI within bursts. $^{**}p < 0.01$ and $^{***}p < 0.001$, compared to Veh; analyzed using one-way ANOVA.

neurotoxic effects by nanoplastics in rodent brains is not well understood (Prust et al., 2020), a comparative analysis between rats and mice is lacking. Our research indicates that PSNPs are predominantly internalized by microglia rather than other brain cells in mice (data not shown), aligning with results from rat cells, suggesting that nanoplastics are primarily internalized by microglia in rodent brains.

The environmental relevance of experimental research on plastic toxicity is a subject of debate (Brito et al., 2022; Rubio et al., 2020). The spherical nanoplastics used in our experiments, while useful for controlled studies, may not fully represent the diverse morphologies of plastics found in natural environments, thus presenting a focused perspective rather than a comprehensive environmental applicability of our results. The heterogeneous morphology of aged plastics in the real world contrasts with the uniform spherical shape of commercially available plastics, which may not accurately represent the characteristics of plastics in the natural environment. The precise amount of nanoplastic exposure in humans is uncertain, and it is likely that humans are exposed to a combined composition of plastics through multiple routes. In contrast, experimental animals are typically exposed to a specific type of plastic at high doses *via* a single route. This study's focus on higher doses yields important insights that augment, rather than precisely replicate, usual human exposure scenarios. Despite this, the ready uptake of smaller particles by cells (Desai et al., 1997; Yong et al., 2020), which may induce more severe toxicity than microplastics, and the lack of comprehensive toxicity information on nanoplastics, necessitate research using specific types of nanoplastics to understand their hazard identification. Subsequent research with larger dose ranges should embrace a wider spectrum of doses to enhance our comprehension of dose-response dynamics and to identify levels where no toxic effects are observed to determine the risk assessment of nanoplastics. Additionally, advanced methods are needed to collect and analyze natural nanoparticles from the environment (Wagner and Reemtsma,

2019).

Behavioral analyses indicate that oral exposure to nanoplastics primarily impairs learning and memory without affecting social interaction, hyperactivity, or anxiety behavior, aligning with previous studies (Jeong et al., 2022; Lee et al., 2023a). The hippocampus, crucial for learning and memory, is particularly vulnerable to oxidative stress (Huang et al., 2015), and the brain's modest antioxidant defenses make it susceptible to oxidative stress (Cobley et al., 2018). Given that microplastics can induce oxidative stress and immune activation (Hu and Palic, 2020), it is plausible that PSNP-induced oxidative stress may selectively inhibit hippocampal neuronal activity, leading to learning and memory deficits.

Recent research employing 3D imaging techniques to visualize plastic internalization offers a more accurate investigation of cellular uptake and the associated toxic mechanisms (Roshanzadeh et al., 2020). The use of 3D imaging has advantages over traditional 2D imaging, specifically in its capacity to differentiate between mere attachment of plastic aggregates to the cellular membrane and actual cellular uptake, shedding light on the mechanisms of cellular specificity. In our study, PSNPs were predominantly internalized by microglia, as confirmed by 3D imaging. Given the link between nuclear morphology and gene expression (Neelam et al., 2020; Skinner and Johnson, 2017), nanoparticles may alter nuclear morphology in astrocytes or neurons, potentially leading to aberrant gene expression.

Microglia, functioning as macrophage-like resident immune cells in the brain, are primarily responsible for phagocytizing exogenous pathogens and facilitating the clearance of cellular debris (Janda et al., 2018). They also play a crucial role in regulating neuroinflammation and wound repair processes (Cherry et al., 2014). Given that phagocytic activities can mediate the internalization of microplastics, leading to altered cellular morphology and cell death (Lam et al., 1993), it is plausible that the phagocytic capacity of microglia facilitates the uptake of PSNPs, which subsequently leads to changes in microglial morphology, activation, and neuroinflammation (Kwon et al., 2022). Moreover, our data demonstrated that neuroinflammation exacerbates the uptake of PSNPs by microglia, highlighting a reciprocal relationship between PSNP uptake and neuroinflammation. Exposure to PSNPs augmented the expression of inflammatory genes in microglia, which are linked to synaptic loss, neuronal death, and pathological conditions in the brain.

DAM are identifiable in specific microglial subsets through single-cell transcriptomic analyses (Keren-Shaul et al., 2017; Krasemann et al., 2017) and are implicated in microglial activation, amoeboid morphology, and phagocytic function (Deczkowska et al., 2018). Given that activated microglia produce excessive inflammatory molecules associated with the initiation and exacerbation of neuropathology (Bachiller et al., 2018), targeting microglial activation is considered a potential therapeutic strategy for neuropathological conditions and neurodegenerative diseases (Varnum and Ikezu, 2012). Activated microglia dysregulate neuronal activity and behaviors and induce neuronal death by releasing soluble factors, such as TNF-α, IL-1β, and IL-6 (Wu et al., 2015). Additionally, the release of C3 and Lcn2 from activated microglia aggravates neuroinflammatory stress (Jung and Ryu, 2023; Wu et al., 2019). Furthermore, microglia exposed to PSNPs exhibited reduced mRNA expression levels of brain-derived neurotrophic factor (BDNF), cAMP response element-binding protein 1 (Creb1), and activating transcription factor 4 (Atf4) (Supplementary Fig. 3). Given that these genes are pivotal regulators of synaptic plasticity, neuronal activity, and hippocampal-dependent learning (Corona et al., 2018; Monteggia et al., 2004), PSNPs likely suppress neurotrophic factors in microglia, contributing to cognitive impairments. Additionally, considering the significant role of microglial BDNF in learning-dependent synapse remodeling and learning behavior (Parkhurst et al., 2013), a reduction in microglial BDNF caused by PSNPs exposure could result in suppressed neuronal activity and deficits in learning and memory functions. Therefore, based on transcriptomic analysis and the rescue effect of inhibitors of microglial activation on neuronal activity, PSNPs induce microglial activation that enhances the release of proinflammatory mediators while suppressing neurotrophic factors, which in turn leads to neuronal suppression or neurotoxicity.

5. Conclusions

Amid growing concerns about the potential brain toxicity from nanoplastic exposure, research into the neurotoxic effects and underlying mechanisms remains nascent. This study has demonstrated that nanoplastics can deposit in the brain following oral ingestion, impairing cognitive functions. Specifically, PSNPs are internalized by microglia, leading to their activation and contributing to suppressed neuronal activity and cognitive deficits. Despite the presence of nanoplastics in the environment and concerns about their environmental implications, their reliable detection and biological impact are either limited or underexplored. Our findings suggest that exposure to nanoplastics may be an environmental factor contributing to cognitive impairments associated with neurodegenerative diseases, primarily through the initiation or exacerbation of microglial activation and neuroinflammation. Future research is crucial to gain a more nuanced understanding of the neurotoxic effects of nanoplastics, especially using sophisticated models that reflect real-world polluted environments. This includes studies involving chronic exposure to plastics, varying particle sizes and morphologies, or combined exposure to different plastics through multiple routes. Such research is vital not only for a comprehensive understanding of the neurotoxic effects of nanoplastics but also for developing effective strategies to mitigate these risks.

Supplementary data to this article can be found online at https://doi.org/10.1016/j.scitotenv.2024.171681.

CRediT authorship contribution statement

Yunn Me Me Paing: Validation, Methodology. **Yunkyung Eom:** Methodology, Investigation. **Gyeong Bae Song:** Formal analysis, Data curation. **Bokyung Kim:** Validation. **Myung Gil Choi:** Investigation. **Sungguan Hong:** Writing – review & editing, Writing – original draft, Supervision, Conceptualization. **Sung Hoon Lee:** Writing – review & editing, Writing – original draft, Supervision, Conceptualization.

Declaration of competing interest

The authors report that there are no competing interests to declare.

Data availability

The datasets used and analyzed during this study are available from the corresponding authors upon reasonable request. The RNA-seq data of microglia exposed to IR-813 or PSNPs were uploaded under the accession GSE 243612.

Acknowledgments

This work was supported by the Korea Environmental Industry and Technology Institute (KEITI) through the Measurement and Risk Assessment Program for Management of Microplastics, funded by the Korea Ministry of Environment (MOE) (Grant No. 2021003120002). Additional support came from a National Research Foundation of Korea (NRF) grant funded by the Korean government (Grant No. 2021R1F1A1062534 and No. 2020R1C1C1008852).

References

Bachiller, S., Jimenez-Ferrer, I., Paulus, A., Yang, Y.Y., Swanberg, M., Deierborg, T., Boza-Serrano, A., 2018. Microglia in neurological diseases: a road map to brain-disease dependent-inflammatory response. Front. Cell. Neurosci. 12, 488. https://doi.org/10.3389/fncel.2018.00488.

Banerjee, A., Shelver, W.L., 2021. Micro- and nanoplastic induced cellular toxicity in mammals: a review. Sci. Total Environ. 755 https://doi.org/10.1016/j.scitotenv.2020.142518.

Barnes, D.K.A., Galgani, F., Thompson, R.C., Barlaz, M., 2009. Accumulation and fragmentation of plastic debris in global environments. Philos. Trans. R. Soc. B 364, 1985–1998. https://doi.org/10.1098/rstb.2008.0205.

Bouwmeester, H., Hollman, P.C.H., Peters, R.J.B., 2015. Potential health impact of environmentally released micro- and nanoplastics in the human food production chain: experiences from nanotoxicology. Environ. Sci. Technol. 49, 8932–8947. https://doi.org/10.1021/acs.est.5b01090.

Brito, W.A.D., Mutter, F., Wende, K., Cecchini, A.L., Schmidt, A., Bekeschus, S., 2022. Consequences of nano and microplastic exposure in rodent models: the known and unknown. Part. Fibre Toxicol. 19 https://doi.org/10.1186/s12989-022-00473-y.

Chae, Y., An, Y.J., 2017. Effects of micro- and nanoplastics on aquatic ecosystems: current research trends and perspectives. Mar. Pollut. Bull. 124, 624–632. https://doi.org/10.1016/j.marpolbul.2017.01.070.

Chen, Q.Q., Gundlach, M., Yang, S.Y., Jiang, J., Velki, M., Yin, D.Q., Hollert, H., 2017. Quantitative investigation of the mechanisms of microplastics and nanoplastics toward zebrafish larvae locomotor activity. Sci. Total Environ. 584, 1022–1031. https://doi.org/10.1016/j.scitotenv.2017.01.156.

Cherry, J.D., Olschowka, J.A., O'Banion, M.K., 2014. Neuroinflammation and M2 microglia: the good, the bad, and the inflamed. J. Neuroinflammation 11, 98. https://doi.org/10.1186/1742-2094-11-98.

Cobley, J.N., Fiorello, M.L., Bailey, D.M., 2018. 13 reasons why the brain is susceptible to oxidative stress. Redox Biol. 15, 490–503. https://doi.org/10.1016/j.redox.2018.01.008.

Colonna, M., Butovsky, O., 2017. Microglia function in the central nervous system during health and neurodegeneration. Annu. Rev. Immunol. 35, 441–468. https://doi.org/10.1146/annurev-immunol-051116-052358.

Corona, C., Pasini, S., Liu, J., Amar, F., Greene, L.A., Shelanski, M.L., 2018. Activating transcription factor 4 (ATF4) regulates neuronal activity by controlling GABA(B)R trafficking. J. Neurosci. 38, 6102–6113. https://doi.org/10.1523/Jneurosci.3350-17.2018.

de Sa, L.C., Oliveira, M., Ribeiro, F., Rocha, T.L., Futter, M.N., 2018. Studies of the effects of microplastics on aquatic organisms: what do we know and where should we focus our efforts in the future? Sci. Total Environ. 645, 1029–1039. https://doi.org/10.1016/j.scitotenv.2018.07.207.

Deczkowska, A., Keren-Shaul, H., Weiner, A., Colonna, M., Schwartz, M., Amit, I., 2018. Disease-associated microglia: a universal immune sensor of neurodegeneration. Cell 173, 1073–1081. https://doi.org/10.1016/j.cell.2018.05.003.

Desai, M.P., Labhasetwar, V., Walter, E., Levy, R.J., Amidon, G.L., 1997. The mechanism of uptake of biodegradable microparticles in Caco-2 cells is size dependent. Pharm. Res. 14, 1568–1573. https://doi.org/10.1023/A:1012126301290.

Ding, J.N., Zhang, S.S., Razanajatovo, R.M., Zou, H., Zhu, W.B., 2018. Accumulation, tissue distribution, and biochemical effects of polystyrene microplastics in the freshwater fish red tilapia (Oreochromis niloticus). Environ. Pollut. 238, 1–9. https://doi.org/10.1016/j.envpol.2018.03.001.

do Sul, J.A.I., Costa, M.F., 2014. The present and future of microplastic pollution in the marine environment. Environ. Pollut. 185, 352–364. https://doi.org/10.1016/j.envpol.2013.10.036.

Edler, M.K., Mhatre-Winters, I., Richardson, J.R., 2021. Microglia in aging and Alzheimer's disease: a comparative species review. Cells 10, 1138. https://doi.org/10.3390/cells10051138.

Estrela, F.N., Guimaraes, A.T.B., Araujo, A.P.D., Silva, F.G., da Luz, T.M., Silva, A.M., Pereira, P.S., Malafaia, G., 2021. Toxicity of polystyrene nanoplastics and zinc oxide to mice. Chemosphere 271, 129476. https://doi.org/10.1016/j.chemosphere.2020.129476.

Ferreira, I., Venancio, C., Lopes, I., Oliveira, M., 2019. Nanoplastics and marine organisms: what has been studied? Environ. Toxicol. Pharmacol. 67, 1–7. https://doi.org/10.1016/j.etap.2019.01.006.

Fonte, E., Ferreira, P., Guilhermino, L., 2016. Temperature rise and microplastics interact with the toxicity of the antibiotic cefalexin to juveniles of the common goby (Pomatoschistus microps): post-exposure predatory behaviour, acetylcholinesterase activity and lipid peroxidation. Aquat. Toxicol. 180, 173–185. https://doi.org/10.1016/j.aquatox.2016.09.015.

Galloway, T.S., Cole, M., Lewis, C., 2017. Interactions of microplastic debris throughout the marine ecosystem. Nat. Ecol. Evol. 1, 116. https://doi.org/10.1038/s41559-017-0116.

Garcia, M.A., Liu, R., Nihart, A., El Hayek, E., Castillo, E., Barrozo, E.R., Suter, M.A., Bleske, B., Scott, J., Forsythe, K., Gonzalez-Estrella, J., Aagaard, K.M., Campen, M.J., 2024. Quantitation and identification of microplastics accumulation in human placental specimens using pyrolysis gas chromatography mass spectrometry. Toxicol. Sci. https://doi.org/10.1093/toxsci/kfae021.

Gigault, J., Halle, A.T., Baudrimont, M., Pascal, P.Y., Gauffre, F., Phi, T.L., El Hadri, H., Grassl, B., Reynaud, S., 2018. Current opinion: what is a nanoplastic? Environ. Pollut. 235, 1030–1034. https://doi.org/10.1016/j.envpol.2018.01.024.

Giridharan, S., Srinivasan, M., 2018. Mechanisms of NF-κB p65 and strategies for therapeutic manipulation. J. Inflamm. Res. 11, 407–419. https://doi.org/10.2147/Jir.S140188.

Grodzicki, W., Dziendzikowska, K., Gromadzka-Ostrowska, J., Kruszewski, M., 2021. Nanoplastic impact on the gut-brain axis: current knowledge and future directions. Int. J. Mol. Sci. 22, 12795 https://doi.org/10.3389/fncel.2021.701673.

Harrison, J.P., Ojeda, J.J., Romero-Gonzalez, M.E., 2012. The applicability of reflectance micro-Fourier-transform infrared spectroscopy for the detection of synthetic microplastics in marine sediments. Sci. Total Environ. 416, 455–463. https://doi.org/10.1016/j.scitotenv.2011.11.078.

Hu, M.Y., Palic, D., 2020. Micro- and nano-plastics activation of oxidative and inflammatory adverse outcome pathways. Redox Biol. 37 https://doi.org/10.1016/j.redox.2020.101620.

Huang, T.T., Leu, D., Zou, Y.N., 2015. Oxidative stress and redox regulation on hippocampal-dependent cognitive functions. Arch. Biochem. Biophys. 576, 2–7. https://doi.org/10.1016/j.abb.2015.03.014.

Hwang, J., Choi, D., Han, S., Jung, S., Choi, J., Hong, J., 2020. Potential toxicity of polystyrene microplastic particles. Sci. Rep. 10 https://doi.org/10.1038/s41598-020-64464-9.

Janda, E., Boi, L., Carta, A.R., 2018. Microglial phagocytosis and its regulation: a therapeutic target in Parkinson's disease? Front. Mol. Neurosci. 11, 144. https://doi.org/10.3389/fnmol.2018.00144.

Jeong, B., Baek, J.Y., Koo, J., Park, S., Ryu, Y.K., Kim, K.S., Zhang, S., Chung, C., Dogan, R., Choi, H.S., Um, D., Kim, T.K., Lee, W.S., Jeong, J., Shin, W.H., Lee, J.R., Kim, N.S., Lee, D.Y., 2022. Maternal exposure to polystyrene nanoplastics causes brain abnormalities in progeny. J. Hazard. Mater. 426, 127815 https://doi.org/10.1016/j.jhazmat.2021.127815.

Jung, B.K., Ryu, K.Y., 2023. Lipocalin-2: a therapeutic target to overcome neurodegenerative diseases by regulating reactive astrogliosis. Exp. Mol. Med. 55, 2138–2146. https://doi.org/10.1038/s12276-023-01098-7.

Katz, R.J., Schmaltz, K., 1980. Dopaminergic involvement in attention a novel animal-model. Prog. Neuropsychopharmacol. 4, 585–590.

Keren-Shaul, H., Spinrad, A., Weiner, A., Matcovitch-Natan, O., Dvir-Szternfeld, R., Ulland, T.K., David, E., Baruch, K., Lara-Astaiso, D., Toth, B., Itzkovitz, S., Colonna, M., Schwartz, M., Amit, I., 2017. A unique microglia type associated with restricting development of Alzheimer's disease. Cell 169, 1276–1290. https://doi.org/10.1016/j.cell.2017.05.018.

Kim, J.S., Yoon, T.J., Kim, B.G., Park, S.J., Kim, H.W., Lee, K.H., Park, S.B., Lee, J.K., Cho, M.H., 2006. Toxicity and tissue distribution of magnetic nanoparticles in mice. Toxicol. Sci. 89, 338–347. https://doi.org/10.1093/toxsci/kfj027.

Kim, S.R., Park, Y., Li, M., Kim, Y.K., Lee, S., Son, S.Y., Lee, S., Lee, J.S., Lee, C.H., Park, H.H., Lee, J.Y., Hong, S.G., Cho, Y.C., Kim, J.W., Yoo, H.M., Cho, N., Lee, H.S., Lee, S.H., 2022. Anti-inflammatory effect of Ailanthus altissima (Mill.) Swingle leaves in lipopolysaccharide-stimulated astrocytes. J. Ethnopharmacol. 286, 114258 https://doi.org/10.1016/j.jep.2021.114258.

Krasemann, S., Madore, C., Cialic, R., Baufeld, C., Calcagno, N., El Fatimy, R., Beckers, L., O'Loughlin, E., Xu, Y., Fanek, Z., Greco, D.J., Smith, S.T., Tweet, G., Humulock, Z., Zrzavy, T., Conde-Sanroman, P., Gacias, M., Weng, Z.P., Chen, H., Tjon, E., Mazaheri, F., Hartmann, K., Madi, A., Ulrich, J.D., Glatzel, M., Worthmann, A., Heeren, J., Budnik, B., Lemere, C., Ikezu, T., Heppner, F.L., Litvak, V., Holtzman, D. M., Lassmann, H., Weiner, H.L., Ochando, J., Haass, C., Butovsky, O., 2017. The TREM2-APOE pathway drives the transcriptional phenotype of dysfunctional microglia in neurodegenerative diseases. Immunity 47, 566–581. https://doi.org/10.1016/j.immuni.2017.08.008.

Kwon, W., Kim, D., Kim, H.Y., Jeong, S.W., Lee, S.G., Kim, H.C., Lee, Y.J., Kwon, M.K., Hwang, J.S., Han, J.E., Park, J.K., Lee, S.J., Choi, S.K., 2022. Microglial phagocytosis of polystyrene microplastics results in immune alteration and apoptosis in vitro and in vivo. Sci. Total Environ. 807, 150817 https://doi.org/10.1016/j.scitotenv.2021.150817.

Lam, K.H., Schakenraad, J.M., Esselbrugge, H., Feijen, J., Nieuwenhuis, P., 1993. The effect of phagocytosis of poly(L-lactic acid) fragments on cellular morphology and viability. J. Biomed. Mater. Res. 27, 1569–1577. https://doi.org/10.1002/jbm.820271214.

Lee, C.W., Hsu, L.F., Wu, I.L., Wang, Y.L., Chen, W.C., Liu, Y.J., Yang, L.T., Tan, C.L., Luo, Y.H., Wang, C.C., Chiu, H.W., Yang, T.C.K., Lin, Y.Y., Chang, H.A., Chiang, Y.C., Chen, C.H., Lee, M.H., Peng, K.T., Huang, C.C.Y., 2023a. Exposure to polystyrene microplastics impairs hippocampus-dependent learning and memory in mice. J. Hazard. Mater. 453, 131398 https://doi.org/10.1016/j.jhazmat.2023.131398.

Lee, S.H., Lin, W.Y., Cheng, T.J., 2023b. Microbiota-mediated metabolic perturbations in the gut and brain of mice after microplastic exposure. Chemosphere 350, 141026. https://doi.org/10.1016/j.chemosphere.2023.141026.

Leyh, J., Paeschke, S., Mages, B., Michalski, D., Nowicki, M., Bechmann, I., Winter, K., 2021. Classification of microglial morphological phenotypes using machine learning. Front. Cell. Neurosci. 15, 701673 https://doi.org/10.3389/fncel.2021.701673.

Liang, B.X., Huang, Y.J., Zhong, Y.Z., Li, Z.M., Ye, R.Y., Wang, B., Zhang, B.L., Meng, H., Lin, X., Du, J.X., Hu, M.J., Wu, Q.H., Sui, H.X., Yang, X.F., Huang, Z.L., 2022. Brain single-nucleus transcriptomics highlights that polystyrene nanoplastics potentially induce Parkinson's disease-like neurodegeneration by causing energy metabolism disorders in mice. J. Hazard. Mater. 430 https://doi.org/10.1016/j.jhazmat.2022.128459.

Materic, D., Holzinger, R., Niemann, H., 2022. Nanoplastics and ultrafine microplastic in the Dutch Wadden Sea - the hidden plastics debris? Sci. Total Environ. 846 https://doi.org/10.1016/j.scitotenv.2022.157371.

Merdy, P., Delpy, F., Bonneau, A., Villain, S., Iordachescu, L., Vollertsen, J., Lucas, Y., 2023. Nanoplastic production procedure for scientific purposes: PP, PVC, PE-LD, PE-HD, and PS. Heliyon 9, e18387. https://doi.org/10.1016/j.heliyon.2023.e18387.

Meyers, J.D., Doane, T., Burda, C., Basilion, J.P., 2013. Nanoparticles for imaging and treating brain cancer. Nanomedicine-UK 8, 123–143. https://doi.org/10.2217/Nnm.12.185.

Mistry, A., Glud, S.Z., Kjems, J., Randel, J., Howard, K.A., Stolnik, S., Illum, L., 2009. Effect of physicochemical properties on intranasal nanoparticle transit into murine olfactory epithelium. J. Drug Target. 17, 543–552. https://doi.org/10.1080/10611860903055470.

Monikh, F.A., Baun, A., Hartmann, N.B., Kortet, R., Akkanen, J., Lee, J.S., Shi, H.H., Lahive, E., Uurasjärvi, E., Tufenkji, N., Altmann, K., Wiesner, Y., Grossart, H.P., Peijnenburg, W., Kukkonen, J.V.K., 2023. Exposure protocol for ecotoxicity testing

of microplastics and nanoplastics. Nat. Protoc. 18, 3534–3564. https://doi.org/10.1038/s41596-023-00886-9.
Monteggia, L.M., Barrot, M., Powell, C.M., Berton, O., Galanis, V., Gemelli, T., Meuth, S., Nagy, A., Greene, R.W., Nestler, E.J., 2004. Essential role of brain-derived neurotrophic factor in adult hippocampal function. Proc. Natl. Acad. Sci. U. S. A. 101, 10827–10832. https://doi.org/10.1073/pnas.0402141101.
Murali, K., Kenesei, K., Li, Y., Demeter, K., Kornyei, Z., Madaraasz, E., 2015. Uptake and bio-reactivity of polystyrene nanoparticles is affected by surface modifications, ageing and LPS adsorption: in vitro studies on neural tissue cells. Nanoscale 7, 4199–4210. https://doi.org/10.1039/c4nr06849a.
Neelam, S., Richardson, B., Barker, R., Udave, C., Gilroy, S., Cameron, M.J., Levine, H.G., Zhang, Y., 2020. Changes in nuclear shape and gene expression in response to simulated microgravity are LINC complex-dependent. Int. J. Mol. Sci. 21, 6762. https://doi.org/10.3390/ijms21186762.
Nikolic, S., Gazdic-Jankovic, M., Rosic, G., Miletic-Kovacevic, M., Jovicic, N., Nestorovic, N., Stojkovic, P., Filipovic, N., Milosevic-Djordjevic, O., Selakovic, D., Zivanovic, M., Seklic, D., Milivojevic, N., Markovic, A., Seist, R., Vasilijic, S., Stankovic, K.M., Stojkovic, M., Ljujic, B., 2022. Orally administered fluorescent nanosized polystyrene particles affect cell viability, hormonal and inflammatory profile, and behavior in treated mice. Environ. Pollut. 305 https://doi.org/10.1016/j.envpol.2022.119206.
Nuruzatulifah, A.M., Nizam, A.A., Ain, N.M.N., 2016. Synthesis and characterization of polystyrene nanoparticles with covalently attached fluorescent dye. Mater. Today Proc. 3, S112–S119. https://doi.org/10.1016/j.matpr.2016.01.015.
Oeckinghaus, A., Ghosh, S., 2009. The NF-κB family of transcription factors and its regulation. Cold Spring Harb. Perspect. Biol. 1 https://doi.org/10.1101/cshperspect.a000034.
Parkhurst, C.N., Yang, G., Ninan, I., Savas, J.N., Yates, J.R., Lafaille, J.J., Hempstead, B. L., Littman, D.R., Gan, W.B., 2013. Microglia promote learning-dependent synapse formation through brain-derived neurotrophic factor. Cell 155, 1596–1609. https://doi.org/10.1016/j.cell.2013.11.030.
Peller, J.R., Mezyk, S.P., Shidler, S., Castleman, J., Kaiser, S., Faulkner, R.F., Pilgrim, C. D., Wilson, A., Martens, S., Horne, G.P., 2022. Facile nanoplastics formation from macro and microplastics in aqueous media*. Environ. Pollut. 313 https://doi.org/10.1016/j.envpol.2022.120171.
Pivokonsky, M., Cermakova, L., Novotna, K., Peer, P., Cajthaml, T., Janda, V., 2018. Occurrence of microplastics in raw and treated drinking water. Sci. Total Environ. 643, 1644–1651. https://doi.org/10.1016/j.scitotenv.2018.08.102.
Prust, M., Meijer, J., Westerink, R.H.S., 2020. The plastic brain: neurotoxicity of micro- and nanoplastics. Part. Fibre Toxicol. 17, 24. https://doi.org/10.1186/s12989-020-00358-y.
Qian, N., Gao, X., Lang, X., Deng, H., Bratu, T.M., Chen, Q., Stapleton, P., Yan, B., Min, W., 2024. Rapid single-particle chemical imaging of nanoplastics by SRS microscopy. Proc. Natl. Acad. Sci. U. S. A. 121, e2300582121 https://doi.org/10.1073/pnas.2300582121.
Rafiee, M., Dargahi, L., Eslami, A., Beirami, E., Jahangiri-rad, M., Sabour, S., Amereh, F., 2018. Neurobehavioral assessment of rats exposed to pristine polystyrene nanoplastics upon oral exposure. Chemosphere 193, 745–753. https://doi.org/10.1016/j.chemosphere.2017.11.076.
Ramsperger, A.F.R.M., Narayana, V.K.B., Gross, W., Mohanraj, J., Thelakkat, M., Greiner, A., Schmalz, H., Kress, H., Laforsch, C., 2020. Environmental exposure enhances the internalization of microplastic particles into cells. Sci. Adv. 6, eabd1211 https://doi.org/10.1126/sciadv.abd1211.
Roshanzadeh, A., Park, S., Ganjbakhsh, S.E., Park, J., Lee, D.H., Lee, S., Kim, E.S., 2020. Surface charge-dependent cytotoxicity of plastic nanoparticles in alveolar cells under cyclic stretches. Nano Lett. 20, 7168–7176. https://doi.org/10.1021/acs.nanolett.0c02463.
Rubio, L., Marcos, R., Hernández, A., 2020. Potential adverse health effects of ingested micro- and nanoplastics on humans. Lessons learned from *in vivo* and *in vitro* mammalian models. J. Toxicol. Environ. Health Part B 23, 51–68. https://doi.org/10.1080/10937404.2019.1700598.
Rummel, C.D., Jahnke, A., Gorokhova, E., Kuhnel, D., Schmitt-Jansen, M., 2017. Impacts of biofilm formation on the fate and potential effects of microplastic in the aquatic environment. Environ. Sci. Technol. Lett. 4, 258–267. https://doi.org/10.1021/acs.estlett.7b00164.
Sandi, C., 2013. Stress and cognition. Wiley Interdiscip. Rev. Cogn. Sci. 4, 245–261. https://doi.org/10.1002/wcs.1222.
Schroter, L., Ventura, N., 2022. Nanoplastic toxicity: insights and challenges from experimental model systems. Small 18, e2201680. https://doi.org/10.1002/smll.202201680.
Schur, C., Rist, S., Baun, A., Mayer, P., Hartmann, N.B., Wagner, M., 2019. When fluorescence is not a particle: the tissue translocation of microplastics in Daphnia magna seems an artifact. Environ. Toxicol. Chem. 38, 1495–1503. https://doi.org/10.1002/etc.4436.
Setala, O., Fleming-Lehtinen, V., Lehtiniemi, M., 2014. Ingestion and transfer of microplastics in the planktonic food web. Environ. Pollut. 185, 77–83. https://doi.org/10.1016/j.envpol.2013.10.013.
Skinner, B.M., Johnson, E.E.P., 2017. Nuclear morphologies: their diversity and functional relevance. Chromosoma 126, 195–212. https://doi.org/10.1007/s00412-016-0614-5.
Steer, M., Cole, M., Thompson, R.C., Lindeque, P.K., 2017. Microplastic ingestion in fish larvae in the western English Channel. Environ. Pollut. 226, 250–259. https://doi.org/10.1016/j.envpol.2017.03.062.
Suman, A., Mahapatra, A., Gupta, P., Ray, S.S., Singh, R.K., 2024. Polystyrene microplastics induced disturbances in neuronal arborization and dendritic spine density in mice prefrontal cortex. Chemosphere 351, 141165. https://doi.org/10.1016/j.chemosphere.2024.141165.
Varnum, M.M., Ikezu, T., 2012. The classification of microglial activation phenotypes on neurodegeneration and regeneration in Alzheimer's disease brain. Arch. Immunol. Ther. Exp. 60, 251–266. https://doi.org/10.1007/s00005-012-0181-2.
Vay, S.U., Flitsch, L.J., Rabenstein, M., Rogall, R., Blaschke, S., Kleinhaus, J., Reinert, N., Bach, A., Fink, G.R., Schroeter, M., Rueger, M.A., 2018. The plasticity of primary microglia and their multifaceted effects on endogenous neural stem cells in vitro and in vivo. J. Neuroinflammation 15, 226. https://doi.org/10.1186/s12974-018-1261-y.
Vaz, V.P., Nogueira, D.J., Vicentini, D.S., Matias, W.G., 2021. Can the sonication of polystyrene nanoparticles alter the acute toxicity and swimming behavior results for Daphnia magna? Environ. Sci. Pollut. Res. 28, 14192–14198. https://doi.org/10.1007/s11356-021-12455-2.
Wagner, S., Reemtsma, T., 2019. Things we know and don't know about nanoplastic in the environment. Nat. Nanotechnol. 14, 300–301. https://doi.org/10.1038/s41565-019-0424-z.
Waring, R.H., Harris, R.M., Mitchell, S.C., 2018. Plastic contamination of the food chain: a threat to human health? Maturitas 115, 64–68. https://doi.org/10.1016/j.maturitas.2018.06.010.
Wu, Y.W., Dissing-Olesen, L., MacVicar, B.A., Stevens, B., 2015. Microglia: dynamic mediators of synapse development and plasticity. Trends Immunol. 36, 605–613. https://doi.org/10.1016/j.it.2015.08.008.
Wu, X.S., Lee, S.H., Sheng, J.S., Zhang, Z., Zhao, W.D., Wang, D.S., Jin, Y.H., Charnay, P., Ervasti, J.M., Wu, L.G., 2016. Actin is crucial for all kinetically distinguishable forms of endocytosis at synapses. Neuron 92, 1020–1035. https://doi.org/10.1016/j.neuron.2016.10.014.
Wu, T., Dejanovic, B., Gandham, V.D., Gogineni, A., Edmonds, R., Schauer, S., Srinivasan, K., Huntley, M.A., Wang, Y.Y., Wang, T.M., Hedehus, M., Barck, K.H., Stark, M., Ngu, H., Foreman, O., Meilandt, W.J., Elstrott, J., Chang, M.C., Hansen, D. V., Carano, R.A.D., Sheng, M., Hanson, J.E., 2019. Complement C3 is activated in human AD brain and is required for neurodegeneration in mouse models of amyloidosis and tauopathy. Cell Rep. 28, 2111–+. https://doi.org/10.1016/j.celrep.2019.07.060.
Xu, E.G.B., Cheong, R.S., Liu, L., Hernandez, L.M., Azimzada, A., Bayen, S., Tufenkji, N., 2020. Primary and secondary plastic particles exhibit limited acute toxicity but chronic effects on. Environ. Sci. Technol. 54, 6859–6868. https://doi.org/10.1021/acs.est.0c00245.
Yang, Q.Y., Dai, H.X., Cheng, Y., Wang, B.L., Xu, J.L., Zhang, Y., Chen, Y.T., Xu, F., Ma, Q.L., Lin, F., Wang, C., 2023. Oral feeding of nanoplastics affects brain function of mice by inducing macrophage IL-1 signal in the intestine. Cell Rep. 42 https://doi.org/10.1016/j.celrep.2023.112346.
Yong, C.Q.Y., Valiyaveettil, S., Tang, B.L., 2020. Toxicity of microplastics and nanoplastics in mammalian systems. Int. J. Environ. Res. Public Health 17, 1509. https://doi.org/10.3390/ijerph17051509.
Yu, P., Liu, Z.Q., Wu, D.L., Chen, M.H., Lv, W.W., Zhao, Y.L., 2018. Accumulation of polystyrene microplastics in juvenile Eriocheir sinensis and oxidative stress effects in the liver. Aquat. Toxicol. 200, 28–36. https://doi.org/10.1016/j.aquatox.2018.04.015.
Zhu, L., Kang, Y.L., Ma, M.D., Wu, Z.X., Zhang, L., Hu, R.X., Xu, Q.J., Zhu, J.Y., Gu, X.H., An, L.H., 2024. Tissue accumulation of microplastics and potential health risks in human. Sci. Total Environ. 915 https://doi.org/10.1016/j.scitotenv.2024.170004.